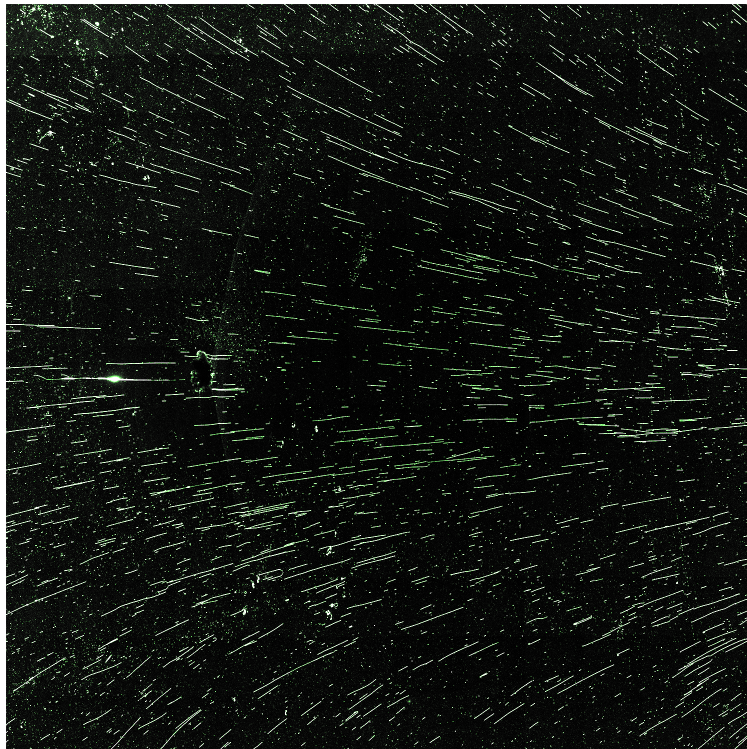




CHALMERS
UNIVERSITY OF TECHNOLOGY



Estimation of Plasmid Lengths on ZEONEX[®]-Coated Cover Slips

Using a Deposinator for Stretching of Single DNA Molecules

Master's thesis in Biomedical Engineering

ALEXANDER RADENKOVIC

MASTER'S THESIS 2017:NN

Estimation of Plasmid Lengths on ZEONEX[®]-Coated Cover Slips

Using a Deposinator for Stretching of Single DNA Molecules

ALEXANDER RADENKOVIC



Department of Biology and Biological Engineering
Division of Chemical Biology
Westerlund Lab
CHALMERS UNIVERSITY OF TECHNOLOGY
Gothenburg, Sweden 2017

Estimation of Plasmid Lengths
on ZEONEX[®]-Coated Cover Slips
Using a Deposinator for Stretching of Single DNA molecules
ALEXANDER RADENKOVIC

© ALEXANDER RADENKOVIC, 2017.

Supervisor: Vilhelm Müller, Department of Biology and Biological Engineering
Examiner: Fredrik Westerlund, Department of Biology and Biological Engineering

Master's Thesis 2017:NN
Department of Biology and Biological Engineering
Division of Chemical Biology
Westerlund Lab
Chalmers University of Technology
SE-412 96 Gothenburg
Telephone +46 31 772 1000

Cover: Plasmid DA255168 cut with S1 nuclease deposited on ZEONEX[®]-coated cover slip using a deposinator

Typeset in L^AT_EX
Gothenburg, Sweden 2017

Abstract

Antibiotic resistance is one of the largest threats to global health, as it counters the way we treat bacterial infections. Antibiotic resistance genes can spread between bacteria via plasmids. Simple and efficient methods for studying plasmids are thus important in the global fight against antibiotic resistance. This project optimizes and evaluates a novel molecular combing method for length estimation of plasmids – dragging a droplet of DNA solution across a ZEONEX[®]-coated cover slip followed by fluorescence microscopy. The method was optimized for pH, deposition speed and concentration using λ -DNA. A plasmid containing the resistance gene *bla_{CTX-M-15}* was linearized using either Cas9 or S1 nuclease, and the efficiency of both endonucleases was assessed. The plasmid was accurately estimated to 150 kbp by using λ -DNA as reference. The method shows promise, but further optimization is required to reduce noise that arise from broken DNA fragments.

Keywords: plasmids, deposinator, molecular combing, Cas9, S1 nuclease.

Acknowledgements

I would like to thank my supervisor, Vilhelm Müller, for all his help despite lack of time, and Hemant Kumar for making the software for extracting and measuring DNA lengths in images. I would further like to thank Fredrik Westerlund and all staff in his group for support and inspiration.

Alexander Radenkovic, Gothenburg, January 2017

Contents

List of Figures	xi
List of Tables	xv
1 Introduction	1
1.1 Relevant Studies	2
2 Theory	3
2.1 DNA & Genetic Information	3
2.1.1 Plasmids	4
2.1.2 λ -DNA	5
2.2 Cas9 and S1 nuclease	5
2.2.1 Cas9 endonuclease	5
2.2.2 S1-nuclease	6
2.3 Fluorescence, Microscopy and Optical Mapping	8
2.3.1 Luminescence	10
2.3.2 YOYO-1	13
2.3.3 Fluorescence Microscopy	13
2.3.4 Optical Mapping	14
2.4 Stepper Motors	14
3 Aim	17
3.1 Project Aim	17
3.1.1 Objectives	17
4 Methods	19
4.1 Preparation and equipment	19
4.1.1 Zeonex coating	19
4.1.2 Deposinator	19
4.1.3 λ -DNA and Plasmid DNA	21
4.1.4 Cleavage of Plasmids Using Cas9 and S1 nuclease	21
4.1.5 Fluorescent staining of DNA	22
4.1.6 Deposition	22
4.1.7 Fluorescence Microscopy	22
4.2 Experimental Setup	22
4.3 Data processing	23
4.3.1 Measuring of single DNA molecules	23

4.3.2	Histogram Plotting	24
5	Results and Discussion	25
5.1	Optimization	25
5.1.1	pH	25
5.1.2	Speed	26
5.1.3	DNA-concentration	26
5.2	Estimation of DNA-length	27
5.2.1	Length of λ -DNA and Non-cut DA25168	27
5.2.2	Length of S1-cut DA25168 and S1-cut DA25168 mixed with λ -DNA	28
5.2.3	Length of DA25168 cut with Cas9	30
5.3	Further Discussion	30
5.3.1	DNA breakage	30
5.3.2	Folding	31
5.3.3	Cas9	31
6	Conclusions	33
	Bibliography	35
A	Protocols	I
A.1	Cas9 Cleavage	I
A.2	S1 nuclease Cleavage	II
B	High Resolution Histograms	III
B.1	Figure 5.3	III
B.2	Figure 5.4	V
B.3	Figure 5.6	VII

List of Figures

2.1	(a) dsDNA in the shape of a double helix [1]. (b) The chemical structure of the two types of base pairs, A connected to T and G connected to C [2, 3]. The dotted lines represent hydrogen bonds.	4
2.2	(a) Chromosome of a eukaryote [4]. (b) Chromosome and plasmid in a bacteria.	5
2.3	The CRISPR loci. The white boxes represent CRISPRs and the colored boxes represent spacer sequences. Each spacer is unique and matches the sequence of various bacteriophages and plasmids. The repeats are followed by a set of <i>cas</i> -genes and are crucial in the CRISPR/Cas system. Reused by permission from Nature Publishing Group [5].	6
2.4	The three types of CRISPR/Cas systems. Type I is matured by either Cas5 or Cas6 and interferes threats together with CRISPR-associated complex for antiviral defense (Cascade) and Cas3. Type II is matured by tracrRNA, RNase II and an unknown factor, and interferes threats together with Cas9. Type III is matured by Cas6 and an unknown factor, and interferes threats together with the Csm/Cmr complex. Reused under creative commons licence [6].	7
2.5	A circular DNA molecule undergoing supercoiling due to either under- or overwinding (left and right respectively) [7].	8
2.6	(a) The energy for different atomic orbitals ranging from 1s to 6s (not to scale and only for comparative purposes). (b) The more primitive Bohr model.	9
2.7	(a) An electron being excited by a photon with energy $h\nu_1$ where $\Delta E = h\nu_1$. (b) An electron returning to the ground state, emitting a photon with energy $h\nu_2$	10
2.8	(a) Fluorescence stemming from the substance quinine when exposed to UV-light [8]. (b) A glow-in-the-dark, phosphorescent toy [9].	11
2.9	The difference between a singlet ground state, a singlet excited state, and a triplet excited state. The horizontal lines represents orbitals and the arrows represents electrons where the direction of the arrows correspond to the angular momentum of each electron, <i>i.e.</i> the direction of their spin.	12

2.10	Jablonski diagram. S_0 refer to the singlet ground state, S_1 and S_2 refers to the first and second singlet excited states respectively, and T_1 refers to the first triplet excited state. At each electronic stage, the system can exist in a number of vibrational states, depicted as horizontal lines. Straight arrows depict radiative decay (or absorption), while swirly arrows depict non-radiative decay.	12
2.11	Chemical structure of YOYO-1 [10]	13
2.12	Schematics of an epifluorescence microscope. Light travels through an excitation filter, removing light not corresponding to the excitation wavelength. The light is led through the objective and excites the sample. The fluorescent light emitted as the sample de-excites is led back through the objective and into an ocular for viewing or camera for image capture. The prefix <i>epi-</i> refers to the fact that the light travels through the objective before exiting the sample, and then travels back though it again. [11]	14
2.13	Four steps of a bipolar stepper motor. In this example, each full rotation consists of 4 steps. The motor consists of a central bar-shaped permanent magnet and four surrounding electromagnets. In step 1, current is led through the coil polarizing the electromagnets on top and below the central magnet. This attracts the two ends of the rod which is thus kept in place. In step 2, current is led through the second coil and the rod shifts 90° clockwise due to magnetic attraction. In step 3, current is led to the first coil again, but this time the direction of current is reversed, thus reversing the polarity of the electromagnets and the central magnet shifts another 90° clockwise. In step 4, current is led through the second coil like in step 2, but with reversed directional flow. The motor then returns to step 1. [12, 13, 14, 15]	15
4.1	Schematics of the deposinator. The stepper motor is controlled by the computer via the circuit board. The translation stage converts the rotational motion of the stepper motor into translational movement of the slider.	20
4.2	Image of the deposinator, including stationary pipette tip.	21
4.3	Early experiments yielded heterogeneous staining which would affect optical mapping.	23
5.1	Results for 0.1 μM λ -DNA in solution with pH 6.1 and 6.5 deposited on ZEONEX [®] -coated cover slips.	25
5.2	0.5 μM (a), 0.25 μM (b), and 0.1 μM (c) λ -DNA deposited on ZEONEX [®] -coated cover slips.	26
5.3	(a) Histogram for the length of λ -DNA deposited on a ZEONEX [®] -coated cover slip. (b) Histogram for the length of non-cut DA25168 deposited on a ZEONEX [®] -coated cover slip. A notable drop at 39 μm has been marked. This is likely about half the length of the plasmid. High resolution versions of both graphs can be found in Appendix B.1.	27

5.4	(a) Histogram for the length of DA25168 cut with S1 nuclease and deposited on ZEONEX [®] -coated cover slip. Notable peaks have been marked with the corresponding lengths. (b) Histogram for the length of λ -DNA mixed with S1-cut DA25168 deposited on ZEONEX [®] -coated cover slip. Notable peaks have been marked with the corresponding lengths. High resolution versions of both graphs can be found in Appendix B.2.	28
5.5	The arrows point to examples of folded DNA molecules. These would likely be regarded as one or two molecules each measured as half the true length. The image is from deposited non-cut DA25168, 0.1 μM	29
5.6	Histogram for the length of DA25168 cut with Cas9 and deposited on ZEONEX [®] -coated cover slip. Notable peaks have been marked with the corresponding lengths. High resolution versions of both graphs can be found in Appendix B.3.	30
5.7	Difference between stretched DA25168 cut with Cas9 or S1 nuclease. Dots appear at the ends of some of the plasmids cut with Cas9. This is likely bundled up DNA which could be due to Cas9 interaction.	32
B.1	High resolution histogram for the length of λ -DNA deposited on ZEONEX [®] -coated cover slip.	III
B.2	High resolution histogram for the length of non-cut DA25168 deposited on ZEONEX [®] -coated cover slip. A notable drop at 39 μm has been marked. This is likely about half the length of the plasmid.	IV
B.3	Histogram for the length of DA25168 cut with S1 nuclease and deposited on ZEONEX [®] -coated cover slip. Notable peaks have been marked with the corresponding lengths.	V
B.4	Histogram for the length of λ -DNA mixed with S1-cut DA25168 deposited on ZEONEX [®] -coated cover slip. Notable peaks have been marked with the corresponding lengths.	VI
B.5	Histogram for the length of DA25168 cut with Cas9 and deposited on ZEONEX [®] -coated cover slip. Notable peaks have been marked with the corresponding lengths.	VII

List of Tables

4.1	Concentrations in the 200x and 10x solutions.	22
4.2	Parameters optimized for deposition of DNA.	23
4.3	The different types of samples that where stretched and analysed . . .	23

1

Introduction

Antibiotic resistant bacteria is a world wide and ever growing problem. It is therefore important to study the way antibiotic resistance spread between bacteria. A way for bacteria to spread antibiotic resistance is through plasmids [16, 17, 18]. These are small, circular DNA molecules that are separate from the chromosomal DNA of the bacteria. Simple and efficient ways of studying plasmids is thus needed in the global fight against antibiotic resistance.

Methods for studying DNA often include fluorescence microscopy. As DNA in solution has a tendency to move and bundle up, such analysis often require fixation and stretching of the DNA molecules. There are several approaches to achieve this, and among these are using nanofluidic channels or molecular combing. Nanofluidic channels allow single DNA molecules in solution to be examined under a microscope in a stretched conformation [19]. The method is efficient for stretching the molecules, but it is quite laborious. Molecular combing involves letting DNA in a solution interact with a positively charged surface [20]. This method stretches the DNA by receding the liquid-surface border [20, 21]. As the DNA leaves the liquid, surface tension stretches the molecules and they remain stretched as they bind to the surface. This can be achieved by placing a cover slip on a positively charged microscope slide. A droplet of DNA solution is then added to the edge of the cover slip, and surface tension pulls the droplet under the cover slip, spreading it across the surface between the microscope slide and the slip. As the liquid evaporates and the surface area of the droplet recedes, the DNA is stretched. This method is simple, but the stretching has often varied directionality, especially when it comes to longer molecules [22].

This project assesses a more sophisticated type of molecular combing technique. ZEONEX[®]-coated cover slips are used for fixation of DNA, and a droplet mechanically dragged across the cover slip is used to achieve the DNA-stretching surface recession. ZEONEX[®] is a polymer with high hydrophobicity that has been utilized for this purpose in similar studies [23]. The method allows for more controlled and repeatable stretching than traditional molecular combing, while using small amounts of DNA sample. In this project, the method was utilized to estimate the length of plasmids. The project is a step in the process of assessing the method for optical mapping, a plasmid characterization method which is explained in Section 2.3.4.

1.1 Relevant Studies

This section describes similar studies on the subject that have been used as guidelines and inspiration. Together with the aim chapter, it also gives the reader a perception of how the project adds to the larger picture of scientific literature.

The plasmids used have previously been linearized using Cas9 by Müller *et al.* (2016) in their study on resistance gene identification. The method used for linearization have been replicated in this project. [24]

Major inspiration has come from Deen *et al.* (2015) when it comes to the deposition of DNA. In their study they assessed a method for deposition of DNA involving dragging a droplet of DNA solution across a polymer-coated cover slip. The polymers tested were ZEONEX[®], PMMA and CYTOP. The study found that using ZEONEX[®]-coated cover slips along with a MES-buffer (pH 5.7) was superior to the other polymers. [23]

Wei *et al.* (2015) demonstrated in a study a way of measuring short (5-48 kbp) DNA molecules. The study utilized molecular combing and a small fluorescence microscope installed on a cell phone to measure the length of the molecules. Their combing technique involved pressing a solution droplet between two cover slips. [25]

Longer DNA molecules, around 8Mbp, were analysed by Kakyov *et al.* (2016). Their combing technique involved perpendicularly pulling a silane-coated glass slide from a DNA-solution [26]. The results were then analysed using fluorescent microscopy [26]. This method could be used to examine the plasmids in this project, but the method requires large amount of DNA solution which might not be possible in cases with limited amount of sample.

2

Theory

This chapter describes the theoretical background necessary for understanding the aim of this project. The structure and function of DNA is presented, as well as the function and application of Cas9 and S1-nuclease, followed by an overview of fluorescence.

2.1 DNA & Genetic Information

In nature, deoxyribonucleic acid (DNA) commonly exists as a double helix – two strands of DNA forming a spiral staircase-like structure (Figure 2.1(a)). This is known as the B form, which was described by James Watson and Francis Crick based on an X-ray diffraction image taken by Rosalind Franklin [27]. The discovery was revolutionary, and today entire fields of science revolve around this molecule of life. This section briefly describes the structure and function of DNA to provide theory for readers not well educated on the subject, or a refreshment for those who are.

A DNA strand is a polymer of repeating monomers known as nucleotides, each nucleotide consisting of two parts. The first part is a sugar (deoxyribose) attached with a phosphate group. It is this part that connects each nucleotide with its neighbour by linkage of the sugar to the neighbouring nucleotide's phosphate group, and is known as the backbone of the molecule. A linear single DNA strand has a 3' terminus and a 5' terminus, where the 3' ends with the sugar of the backbone, and the 5' ends with the phosphate group of the backbone. The second part of the nucleotide is a base; this base may be either adenine (A), thymine (T), guanine (G) or cytosine (C), and the order of these bases along the DNA strand defines the genetic information present in the molecule. In a double-stranded DNA molecule (dsDNA) it is these bases that, through hydrogen bonds, connect the two strands to each other. However, each base-type only binds to one of the other base-types – A only binds to T, and G only binds to C (Figure 2.1(b)). Such bases are said to be complementary to each other and two complementary bases are known as a base pair. Each base pair in a dsDNA molecule must be complementary for the two strands to be bound together. As a note, however, there are cases where the dsDNA keeps affinity despite minor discrepancies to the complementary sequence. [28]

DNA stores the genetic information in all living organisms. The As, Ts, Gs and Cs line up along the DNA to form sequences called genes. Each gene codes for a protein with specific function, and the complete set of genes in an organism is called its genome. Since humans spawn new offspring through sexual reproduction, every

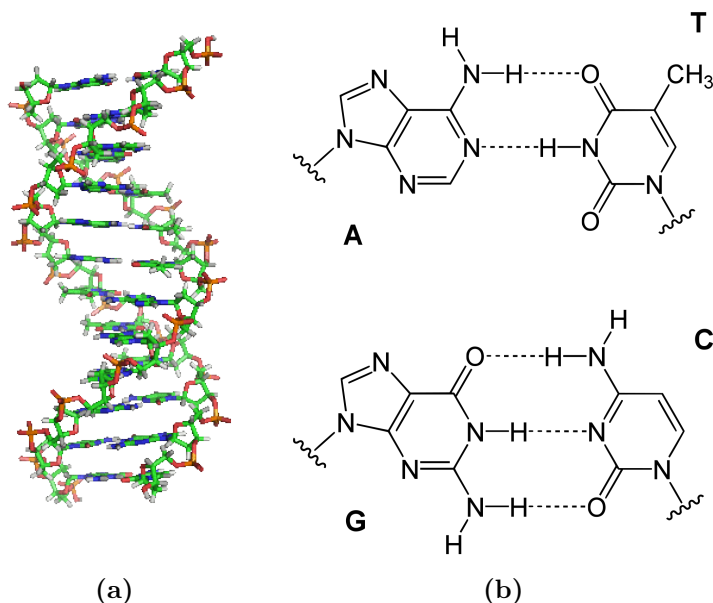


Figure 2.1: (a) dsDNA in the shape of a double helix [1]. (b) The chemical structure of the two types of base pairs, A connected to T and G connected to C [2, 3]. The dotted lines represent hydrogen bonds.

child's genome is a combination of her parents'. Human beings thus gain hereditary traits from their parents, which is why you are more likely to resemble your sibling than your cousin. [28]

All organisms store their DNA in small packages known as chromosomes. Eukaryotic organisms (*e.g.* animals, plants and fungi) have two or more chromosomes, and store their DNA in linear bundles. Bacteria, as opposed to eukaryotes, each have a single chromosome where the DNA is stored as circular DNA, meaning that the two ends of the molecule are connected, forming a ring. Figure 2.2 shows the difference between eukaryotic and bacterial chromosomes. [28]

2.1.1 Plasmids

Many bacteria contain extra genetic information in additional circular DNA molecules, separate from the chromosome. These are called plasmids, and they can be replicated and transferred between different bacteria. Plasmids are part of what makes bacteria so adaptable, and allow spreading of antibiotic resistance. Cases of bacteria with plasmids containing resistance genes are numerous, and make plasmids an important part of studying antibiotic resistance [16, 17, 18, 29].

Traditionally, plasmids are studied using gel electrophoresis [30, 31]. However, this does not study single molecules, and sequence characterization is not possible in the same way as it is for optical mapping. Another common method for analysing plasmids is PCR [32].

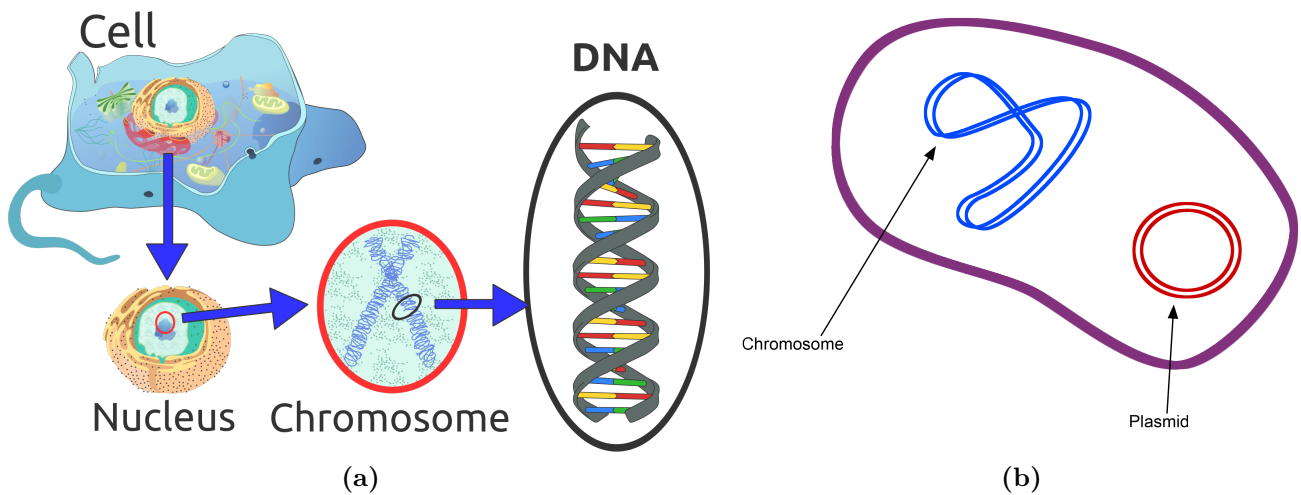


Figure 2.2: (a) Chromosome of a eukaryote [4]. (b) Chromosome and plasmid in a bacteria.

2.1.2 λ -DNA

Enterobacteria phage λ is a bacteriophage common in *E. coli*. The genome is 48.5 kbp long and codes for 12-14 proteins [33]. This genome is often used as model DNA, is commercially available, and will in this project be used as reference.

2.2 Cas9 and S1 nuclease

The ability to cut DNA at specific locations is important for various reasons. It makes it possible to, for example, provide information about genetic information present in the DNA or to even change this information. Cutting of DNA is done using endonucleases, which are enzymes that cleave phosphodiester bonds in the backbone of the molecule. These enzymes are often guided to specific sequences in the DNA, and it is thus possible to cut DNA in specifically targeted regions. This project utilizes endonucleases for linearization of plasmids, and this section describes how to achieve this using CRISPR associated protein 9 (Cas9) and S1-nuclease.

2.2.1 Cas9 endonuclease

Cas9 is part of the adaptive CRISPR/Cas immune system found in many bacteria and archaea [5, 34]. The CRISPR/Cas system provides protection against various bacteriophages and plasmids, and was first discovered in *E. coli* [5, 6]. The system is today often used for insertion of genetic information in DNA molecules.

CRISPR stands for Clustered Regularly Interspaced Short Palindromic Repeats. These are short repetitions of DNA which are separated by short spacer sequences [5, 6, 34]. Spacer DNA is non-coding DNA that most often does not contain any genetic information. However, the spacer sequences between CRISPRs match sequences of infecting bacteriophages or plasmids [5, 6, 34]. When a new bacteriophage or plasmid infects the host, new spacer sequences can be acquired to match the current threat – this is what makes the system so adaptable [5, 6, 34].

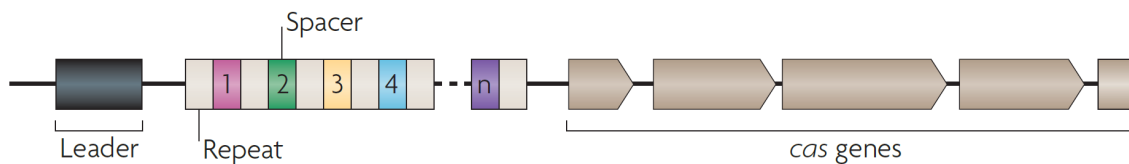


Figure 2.3: The CRISPR loci. The white boxes represent CRISPRs and the colored boxes represent spacer sequences. Each spacer is unique and matches the sequence of various bacteriophages and plasmids. The repeats are followed by a set of *cas*-genes and are crucial in the CRISPR/Cas system. Reused by permission from Nature Publishing Group [5].

The mechanism of addition of new spacers is unknown, but one possibility is that Cas1 plays an important role [5]. CRISPRs are generally preceded by a leader sequence, and followed by a number of *cas*-genes [35]. This is known as the CRISPR loci which is depicted in Figure 2.3

The CRISPR/Cas system works in three stages [6]. The first stage is adaption, where new spacers are inserted into the CRISPR locus [6]. When a new spacer has been added to the CRISPR, it provides specificity for the CRISPR/Cas immune system [5]. The second stage is expression, where the *cas*-genes are expressed and a long precursor CRISPR RNA (crRNA) is transcribed from the CRISPRs and its spacers [5, 6, 34]. This precursor is processed by a Cas protein, which results in small crRNAs [5]. The last stage is interference, where a Cas protein complex work by guidance of crRNA to destroy the targeted nucleic acids of the invader [5, 6, 34].

There are three types of CRISPR/Cas systems: Type I, II and III (Figure 2.4). The type relevant for this project is Type II, where crRNA maturation is dependent on host RNase II and base-pair binding of a trans-coded small RNA (tracrRNA) [6]. Interference of the invading phage or plasmid in Type II systems works through Cas9, which binds to the crRNA and tracrRNA and cleaves DNA by guidance of the crRNA [6]. The Type II CRISPR/Cas system is today utilized for targeted cleavage of DNA in laboratory experiments [36, 37, 38].

In a study by Müller *et al.* (2016), the Type II CRISPR/Cas system was used in combination with optical mapping to directly target and identify antibiotic resistance in plasmids [24]. CRISPR/Cas was specifically used to target and cut plasmids into their linear configuration. This method of plasmid linearization has been mimicked and utilized in this project.

2.2.2 S1-nuclease

S1 nuclease is derived from the fungus *Aspergillus oryzae* and cleaves single stranded DNAs and RNAs into oligonucleotides or mononucleotides [39]. However, S1 nuclease can also be used to linearize large plasmids [40]. Circular DNA can undergo supercoiling, as depicted in Figure 2.5. Supercoiled DNA is more sensitive to enzymes than non-supercoiled, which allows S1 nuclease to linearize the DNA [40, 41, 42]. This works in two steps. Firstly, S1 nuclease induces a nick on one of the strands in the supercoiled circular DNA, which relaxes the molecule to a nicked circular DNA molecule [42]. Secondly, the enzyme cleaves the DNA molecule opposite the nick as this region is now single-stranded [42]. This results is a linear double-stranded DNA

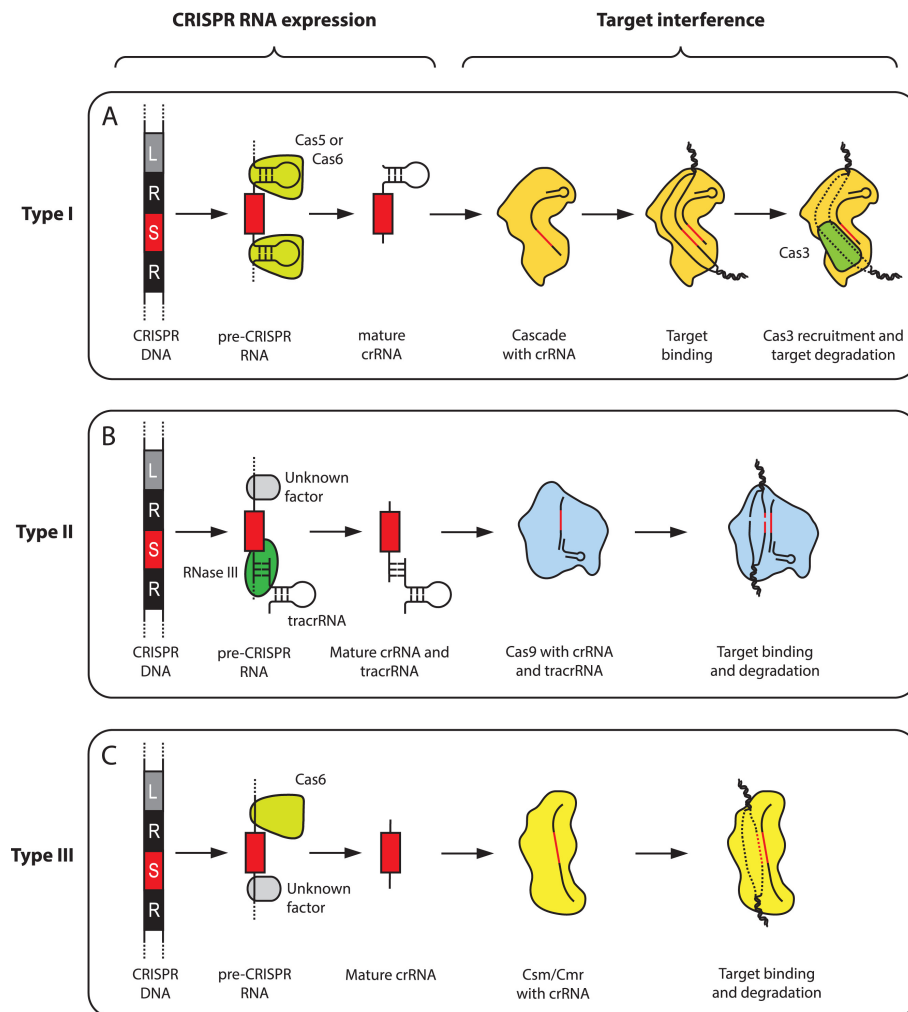


Figure 2.4: The three types of CRISPR/Cas systems. Type I is matured by either Cas5 or Cas6 and interferes threats together with CRISPR-associated complex for antiviral defense (Cascade) and Cas3. Type II is matured by tracrRNA, RNase II and an unknown factor, and interferes threats together with Cas9. Type III is matured by Cas6 and an unknown factor, and interferes threats together with the Csm/Cmr complex. Reused under creative commons licence [6].

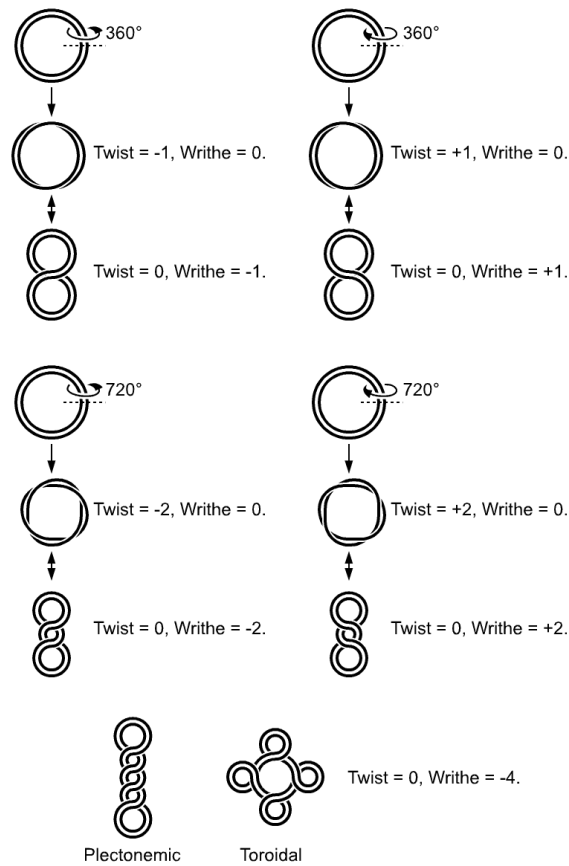


Figure 2.5: A circular DNA molecule undergoing supercoiling due to either under- or overwinding (left and right respectively) [7].

molecule.

In this project, S1 nuclease will be used for linearization of plasmids. It will serve as an easier but less accurate method for linearizing plasmids than usage of CRISPR/Cas9.

2.3 Fluorescence, Microscopy and Optical Mapping

There are various ways of studying DNA, but many rely on staining with fluorescent compounds. This section describes the physics and history behind fluorescence and how it can be used for DNA analysis.

All type of light is made up of photons, small particles – or waves – of energy. The energy of a photon is proportional to its frequency according to the Planck-Einstein relation (Equation 2.1).

$$E = h \cdot \nu \tag{2.1}$$

where E is the energy of the photon, h is Planck's constant and ν is the photon's frequency. There are various ways that a substance can emit light. Traditional light

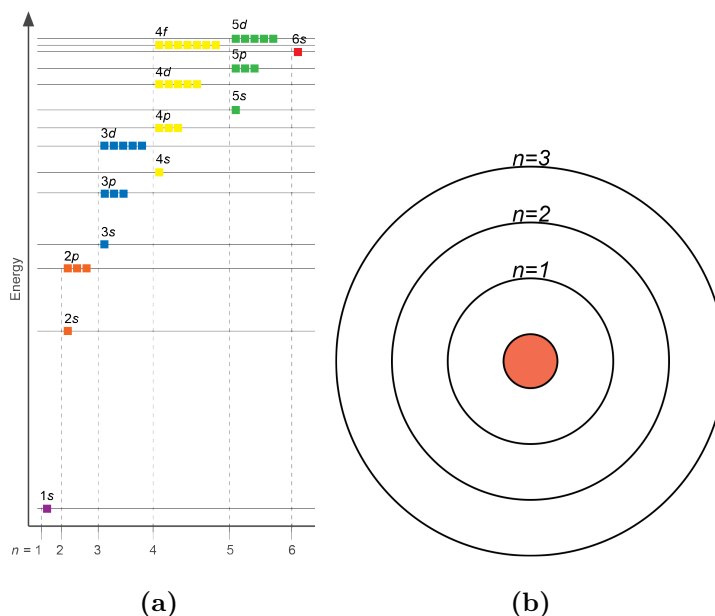


Figure 2.6: (a) The energy for different atomic orbitals ranging from $1s$ to $6s$ (not to scale and only for comparative purposes). (b) The more primitive Bohr model.

bulbs, for example, emit light through incandescence, which occurs when a substance emits light due to high temperature. Fluorescence works differently, and to understand the underlying physics of the phenomenon it is important to understand the physics of atoms and molecules.

An atom consists of a nucleus containing protons and neutrons. Orbiting this nucleus are a number of electrons matching the number of protons. Electrons spin around an axis and each has a spin quantum number of either $1/2$ or $-1/2$, which describes the angular momentum of the electron. The wave-like behaviour of electrons in an atom, molecule or ion are described by distribution functions known as orbitals, each containing up to two electrons. Each orbital is denoted by an energy level, n , and what type of orbital it is. The different types of atomic orbitals are s , p , d and f . Electrons in an atom always fill low energy orbitals before they fill higher ones. Hydrogen has one electron in the lowest energy orbital, as it is the only electron the atom has. This orbital is known as the $1s$ -orbital. Helium also only has electrons in the $1s$ -orbital, as the atom only has two electrons. Continuing along the periodic table, however, more orbitals are filled as the number of electrons increases. The next orbital in order is $2s$ – the number 2 implies that the orbital is at an energy level above $1s$. These energy levels can be compared to the atomic shells of the more primitive Bohr model (Figure 2.6). Molecules have orbitals just like atoms, but these are instead combinations of the atomic ones. Molecular orbitals are denoted σ and π . [43, 44]

In quantum mechanics, electronic states refer to discrete values of energy that electrons in an atom, molecule or ion can take on. If all electrons of an atom, molecule or ion only occupy the lowest energy orbitals, the system is said to be in its ground state. If enough energy is added to the system, an electron can transition to a higher energy orbital. The electron is then referred to as excited, and the system is now in an excited state. For an electron in the system to be excited

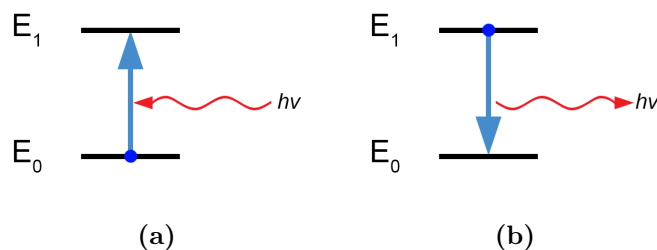


Figure 2.7: (a) An electron being excited by a photon with energy $h\nu_1$ where $\Delta E = h\nu_1$. (b) An electron returning to the ground state, emitting a photon with energy $h\nu_2$.

to a higher state, the added energy needs to be the same as the energy difference between the two levels (Figure 2.7(a)). For example, if the excitation is due to a photon (photoexcitation), the energy of the photon needs to correspond to the levels' difference in energy ($\Delta E = E_1 - E_0 = h\nu$). If an electron returns to the ground state after excitation, it might emit energy in the form of a photon (Figure 2.7(b)) – a phenomenon known as luminescence. [43, 44]

2.3.1 Luminescence

Luminescence occurs when a substance emits light due to relaxation of excited electronic states [45, 46]. This is thus, as opposed to incandescence, not due to high temperature of the substance [45] – hot, glowing metal or molten lava is for example not luminescent. The term luminescence was first introduced by Eilhard Wiedemann in 1888 [45, 47]. As this was some years before quantum theory, Wiedemann was naturally unaware of the existence of excited electronic states. His definition of luminescence was thus “Eine terminologie für die Lichterscheinungen, die nicht durch eine temperaturerhöhung allein bedingt sind”, roughly translated into “A terminology for light appearances which are not caused by a temperature increase alone” [47]. A more current definition can be found in *Glossary of terms used in photochemistry* (2007) as a “Spontaneous emission of radiation from an electronically excited species or from a vibrationally excited species not in thermal equilibrium with its environment” [48]. Different types of luminescence are categorized depending on the mode of excitation; examples include photoluminescence, chemiluminescence and bioluminescence [45]. The form of luminescence relevant to this thesis is photoluminescence which is defined as “luminescence arising from direct photoexcitation of the emitting species” [48].

Photoluminescence is divided into two sub-categories, fluorescence and phosphorescence (Figure 2.8). Photoluminescent substances are placed in these categories based on the nature of the excited state [45, 46]. The difference between fluorescence and phosphorescence was previously based on the duration of the emission [45]. Fluorescent emission was thought to stop simultaneously with the end of excitation, and phosphorescent emission was thought to last longer. Although phosphorescence in most cases lasts longer than fluorescence, the difference is today described by singlet excited states and triplet excited states [46].

A system exists in a singlet or triplet state depending on the multiplicity of

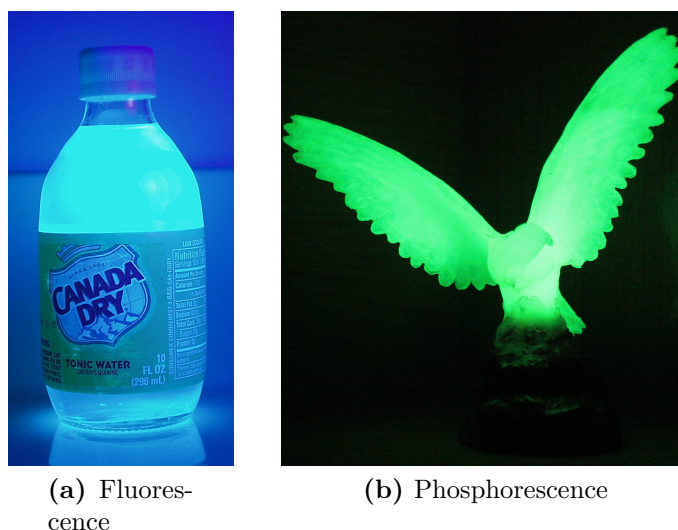


Figure 2.8: (a) Fluorescence stemming from the substance quinine when exposed to UV-light [8]. (b) A glow-in-the-dark, phosphorescent toy [9].

the system. Multiplicity is defined by Equation 2.2 and corresponds to the number of possible orientations of the system's spin angular momentum.

$$Multiplicity = 2 \cdot S + 1 \quad (2.2)$$

where S stands for the total spin quantum number. The multiplicity depends in turn on the total spin quantum number, which describes the intrinsic angular momentum of a particle. Two paired electrons in an orbital have opposite spins, meaning they have a spin quantum number of $1/2$ and $-1/2$ respectively. As the orbital thus has a total spin quantum number of 0 the multiplicity of the atom or molecule, if all other electrons also are paired, equals to $2 \cdot 0 + 1 = 1$. This is known as a singlet state. An unpaired electron instead has the multiplicity of 2 , and thus exists in a doublet state. If a system has two unpaired electrons with the same spin quantum number, the multiplicity equals 3 , which is a triplet state. As opposed to the singlet states, the two electrons in the triplet excited state are not paired. [44, 49]

As an example, consider Figure 2.9. The horizontal lines represent orbitals, and the arrows represent electrons with different spin. In the first case, the electrons have opposite spin, resulting in a total spin quantum number of $1/2 + (-1/2) = 0$. The multiplicity is thus $2 \cdot 0 + 1 = 1$, and the system is in a singlet state. As none of the electrons are excited, the system is also in the ground state. In the second case, the electrons still have opposite spins, but one of the electrons is excited to a higher energy level orbital. This system is thus in a singlet excited state. In the last case, the excited electron has the same spin as the non-excited one, resulting in a total spin quantum number of $1/2 + 1/2 = 1$. The multiplicity is thus $2 \cdot 1 + 1 = 3$, and the system is in a triplet state. This would thus be referred to as a triplet excited state. [44, 49]

How all this relates to fluorescence and phosphorescence can be seen in a Jablonski diagram as depicted in Figure 2.10. When light absorption occurs, the molecule is usually excited to either S_1 or S_2 . If the molecule is excited to S_2 , it al-

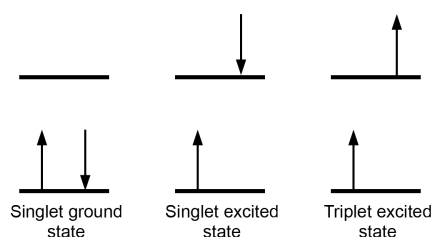


Figure 2.9: The difference between a singlet ground state, a singlet excited state, and a triplet excited state. The horizontal lines represent orbitals and the arrows represent electrons where the direction of the arrows corresponds to the angular momentum of each electron, *i.e.* the direction of their spin.

most always rapidly relaxes to the lowest level of S_1 through non-radiative processes known as vibrational relaxation and internal conversion. Vibrational relaxation occurs when the molecule relaxes to lower vibrational levels of the same excited state by giving away energy as heat. Internal conversion occurs when a molecule transitions from a higher state to a lower, while retaining its molecular spin. This can occur when the vibrational levels of different states overlap. From S_1 , the system may return to the ground state through fluorescence, emitting light. [46] If not, the system returns to the ground state non-radiatively by internal conversion. Many excited substances return to the ground state by a combination of luminescence and internal conversion.

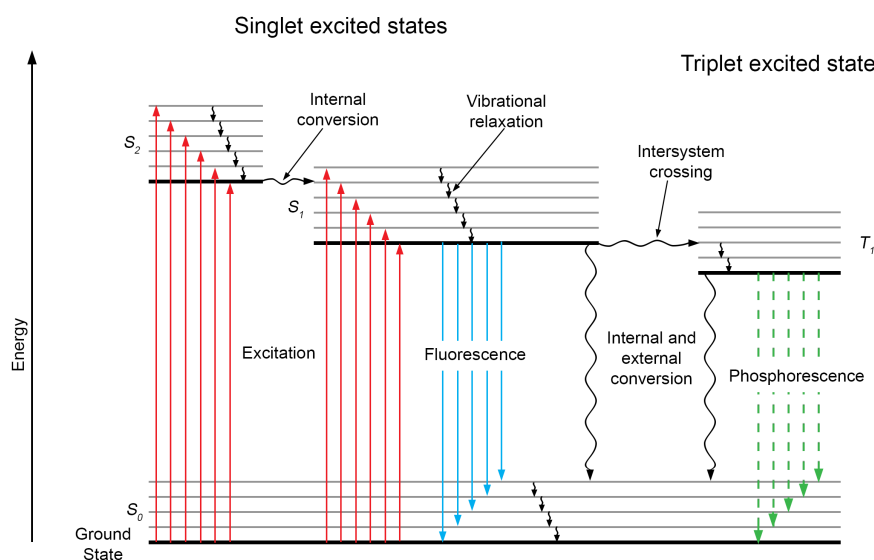


Figure 2.10: Jablonski diagram. S_0 refers to the singlet ground state, S_1 and S_2 refer to the first and second singlet excited states respectively, and T_1 refers to the first triplet excited state. At each electronic stage, the system can exist in a number of vibrational states, depicted as horizontal lines. Straight arrows depict radiative decay (or absorption), while swirly arrows depict non-radiative decay.

Instead of returning to the ground state, the molecule may undergo intersystem crossing between S_1 and T_1 . This occurs when the excited electron reverses spin, and is more likely to happen when the vibrational levels of the two states overlap. From T_1 , the molecule can then return to the ground state through phosphorescence, emitting light. The molecule can also return to the ground state from T_1 through internal conversion, just like with S_1 , without emitting any light. A molecule can undergo excitation directly to a triplet excited state, but due to the additional spin-reversal it is highly unlikely. To sum up, fluorescence occurs from a singlet excited state, and phosphorescence occurs from a triplet excited state. [46]

2.3.2 YOYO-1

Fluorescent compounds are called fluorophores. A common fluorophore for staining DNA is YOYO-1 [50, 51, 52], which is a homodimeric derivate of the oxazole yellow dye [53]. The chemical name of YOYO-1 is 1,1'-(4,4,8,8-tetramethyl-4,8-diazaundecamethylene)bis[4-[(3-methylbenzo-1,3-oxazol-2-yl)methylidene]-1,4-dihydroquinolinium] tetraiodide [53]. As this is somewhat of a mouthful, the naming convention of YOYO-1 is based on the abbreviation of oxazole yellow (YO), and the fact that it is a dimer of YO [53]. Figure 2.11 shows the chemical structure of YOYO-1.

YOYO-1's popularity when it comes to staining of DNA stems from four properties of the compound: It binds well to DNA, it is strongly fluorescent when bound to DNA, it is non-fluorescent in solution, and it has a high molar attenuation coefficient (relates to the absorptivity of the compound) [53]. YOYO-1 binds to DNA through *bis*-intercalation between adjacent base pairs, of double stranded DNA [54].

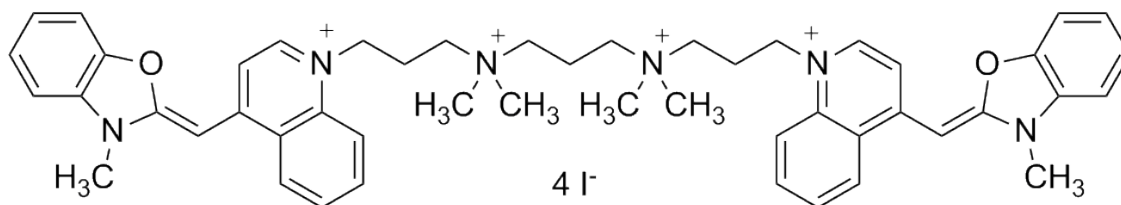


Figure 2.11: Chemical structure of YOYO-1 [10]

2.3.3 Fluorescence Microscopy

The phenomenon of fluorescence can be used to study small, otherwise non-discernable molecules under a microscope. This project utilizes epifluorescence microscopy for imaging of DNA molecules.

Each type of fluorophore is excited by different wavelengths. A fluorescence microscope thus works by exciting the fluorophore with light of the corresponding wavelength. As the substance de-excites, fluorescent light is led through the objective of the microscope, allowing observation. As each fluorophore also emits light of a certain wavelength, a filter in the microscope is used to reduce unwanted emission. Figure 2.12 shows the schematics of an epifluorescent microscope. The fluorophore

used in this project, YOYO-1, is excited by the wavelength 491 nm , and emits light at 509 nm [55].

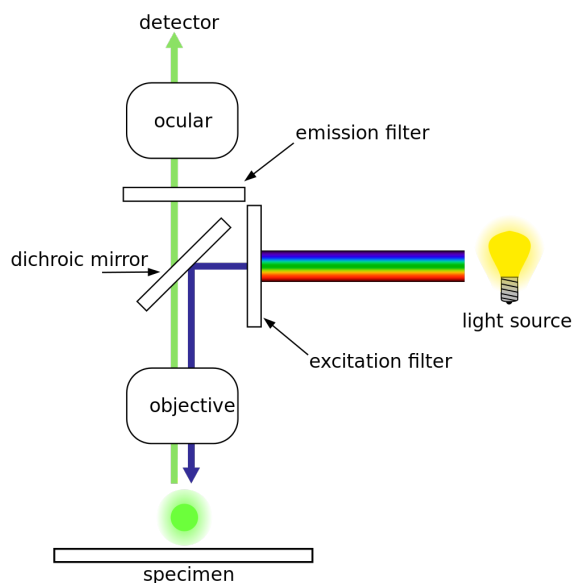


Figure 2.12: Schematics of an epifluorescence microscope. Light travels through an excitation filter, removing light not corresponding to the excitation wavelength. The light is led through the objective and excites the sample. The fluorescent light emitted as the sample de-excites is led back through the objective and into an ocular for viewing or camera for image capture. The prefix *epi-* refers to the fact that the light travels through the objective before exiting the sample, and then travels back through it again. [11]

2.3.4 Optical Mapping

There are various ways of studying genes and sequences of DNA. One way is optical mapping, which provides information about the sequence of single DNA molecules. Optical mapping does not provide the exact sequence of a molecule, but instead provides a barcode that reflects the sequence. This barcode can provide sequence specific information about a DNA molecule, such as deletions and insertions. [19, 22]

One way of generating these barcodes is utilizing YOYO-1 in combination with netropsin, an antibiotic from *Streptomyces Netropsin*. The method works via competitive binding; as netropsin binds with high affinity to AT-rich regions, staining of YOYO-1 in those regions is restricted. When studied under fluorescence microscope, the AT-rich regions of the molecule will have a lower fluorescence than the GC-rich regions. This yields a fluorescent pattern along the DNA molecule depending on its sequence, and can be used to extract information about the molecule. [19, 22, 56, 57]

Optical DNA mapping has been used in combination with the CRISPR/Cas system to study antibiotic resistance in bacteria. [24]

2.4 Stepper Motors

Stepper motors are high precision electric motors that divide a full rotation into a number of steps. There are unipolar and bipolar stepper motors. This project

utilizes a bipolar motor, and its function is explained in this section.

The function of a simple 4 step bipolar stepper motor is shown in Figure 2.13. The motor consists of a central bar-shaped permanent magnet and four surrounding electromagnets. By leading current through the electromagnets in specific conceptions, the central magnet is induced to rotate.

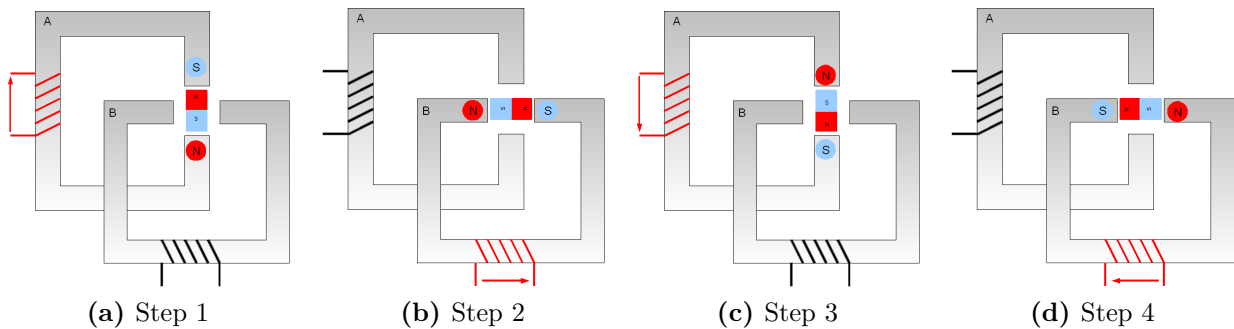


Figure 2.13: Four steps of a bipolar stepper motor. In this example, each full rotation consists of 4 steps. The motor consists of a central bar-shaped permanent magnet and four surrounding electromagnets. In step 1, current is led through the coil polarizing the electromagnets on top and below the central magnet. This attracts the two ends of the rod which is thus kept in place. In step 2, current is led through the second coil and the rod shifts 90° clockwise due to magnetic attraction. In step 3, current is led to the first coil again, but this time the direction of current is reversed, thus reversing the polarity of the electromagnets and the central magnet shifts another 90° clockwise. In step 4, current is led through the second coil like in step 2, but with reversed directional flow. The motor then returns to step 1. [12, 13, 14, 15]

The motor utilized in this project has a somewhat more complex nature, but the principle remains the same. Instead of a rod, there is a solid cylinder with several magnets on the outside, called teeth. By increasing the number of teeth around the central cylinder, the rotation of each step is decreased. The stepper motor in this project has 100 teeth, which yields 400 steps during a full rotation. Each step thus results in a 0.9° rotation.

3

Aim

3.1 Project Aim

The general aim of this project is to assess the use of ZEONEX[®]-coated cover slips and fluorescence microscopy for length estimation of plasmids. This project is part of a larger aim – to utilize the DNA stretching method for optical mapping of single DNA molecules.

3.1.1 Objectives

The project aims to evaluate and optimize a DNA-measuring protocol for estimation of plasmid lengths. A device for dragging a droplet containing DNA molecules on ZEONEX[®]-coated cover slips will be used. The dragging of the droplet should fixate and stretch the molecules, allowing image capture with fluorescence microscopy. The following parameters will be optimized: moving the droplet at different speeds, concentration of DNA in the droplet, and pH of the solution. Further, data received from plasmids cleaved using S1 nuclease or Cas9 endonuclease will be compared to non-cleaved plasmids. The length of stretched plasmids will be compared to the stretched length of λ -DNA in order to calculate the size of the plasmid. This value will be compared to the true size of the plasmid to assess the accuracy of the method.

3. Aim

4

Methods

This chapter describes the methods utilized in this project. The first section goes through preparations necessary for collection of data, the second goes through the experimental setup, and the last section describes post processing of data.

4.1 Preparation and equipment

Necessary preparations for collection of data are described in this section along with function and mechanisms of utilized equipment.

4.1.1 Zeonex coating

ZEONEX[®] is a highly hydrophobic polymer from the company ZEON. It is used in this project due to the successful results with the polymer in the study by Deen *et al.* [23].

A 0.175 g piece of ZEONEX[®] was dissolved in 11.667 ml chlorobenzene to obtain a 1.5% w/v ZEONEX[®] solution. The dissolution took about three hours, whereupon the solution was separated into 2 ml glass vials and stored at room temperature. A glass cover slip was placed on a spin coater and 30-40 μ l ZEONEX[®] solution was added on top. The cover slip was then spun at 3000 rpm for 90 s. To smoothen the surface, the cover slips were heated at 120° C for 1 h immediately after coating. Coated cover slips were stored at room temperature in petri dishes sealed with Parafilm M[®]. The bottom of the petri dishes were covered with a lens paper to facilitate retrieval of the cover slips when intended for use.

4.1.2 Deposinator

Deen *et al.* initially proposed and utilized this setup, and it has in this project been assembled according to their instructions.

The deposinator consists of three parts: an RS Pro hybrid stepper motor (0.9°, 400 steps), a translation stage, and an Arduino UNO circuit board connected to a computer. The slider moves back or forward by activation of the stepper motor which is controlled by the Arduino board. This works by the translation stage which converts the rotational motion of the motor into translational motion of the slider. The computer software was made by Deen *et al.*, and allowed for three different speeds denoted fast, medium and slow. The speeds corresponded to 2, 10 and 60 rpm respectively, where rpm relates to the rotation of the stepper motor. 1 full

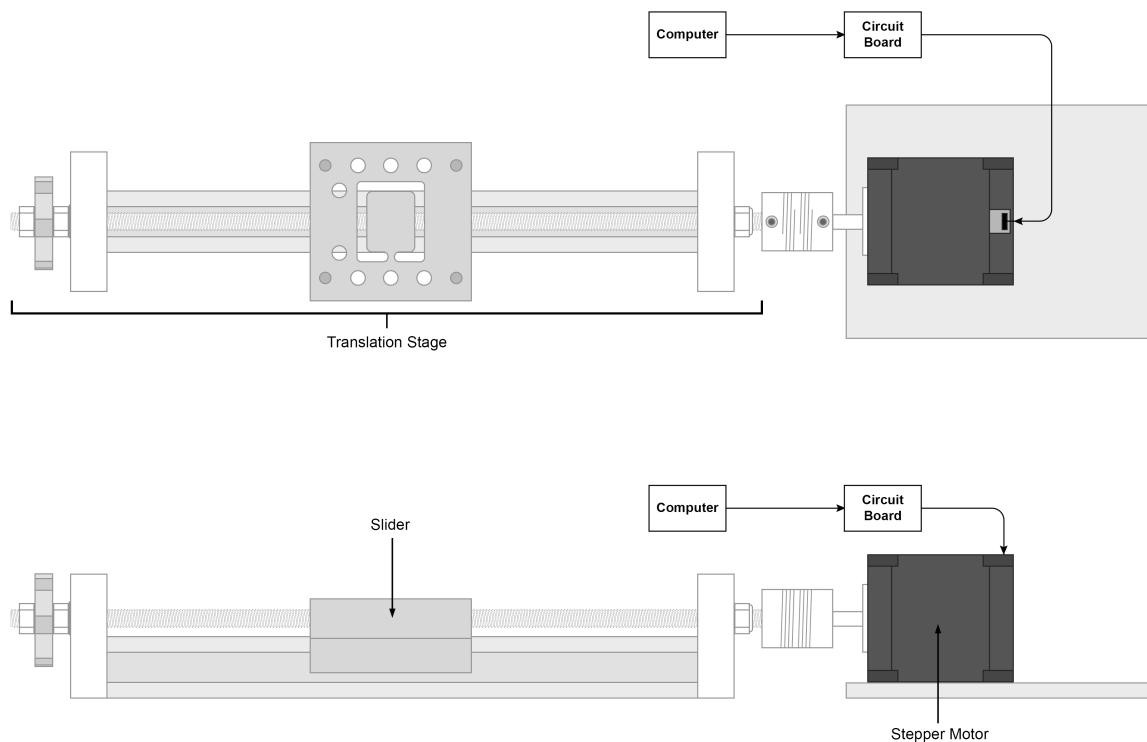


Figure 4.1: Schematics of the depositor. The stepper motor is controlled by the computer via the circuit board. The translation stage converts the rotational motion of the stepper motor into translational movement of the slider.

rotation of the stepper motor was converted to 1 mm movement of the slider. The three motor speeds thus correspond to 2, 10 and 60 mm/min of deposition speed. Figure 4.1 shows schematics of the depositor, and Figure 4.2 shows an image of it, including the stationary pipette tip.

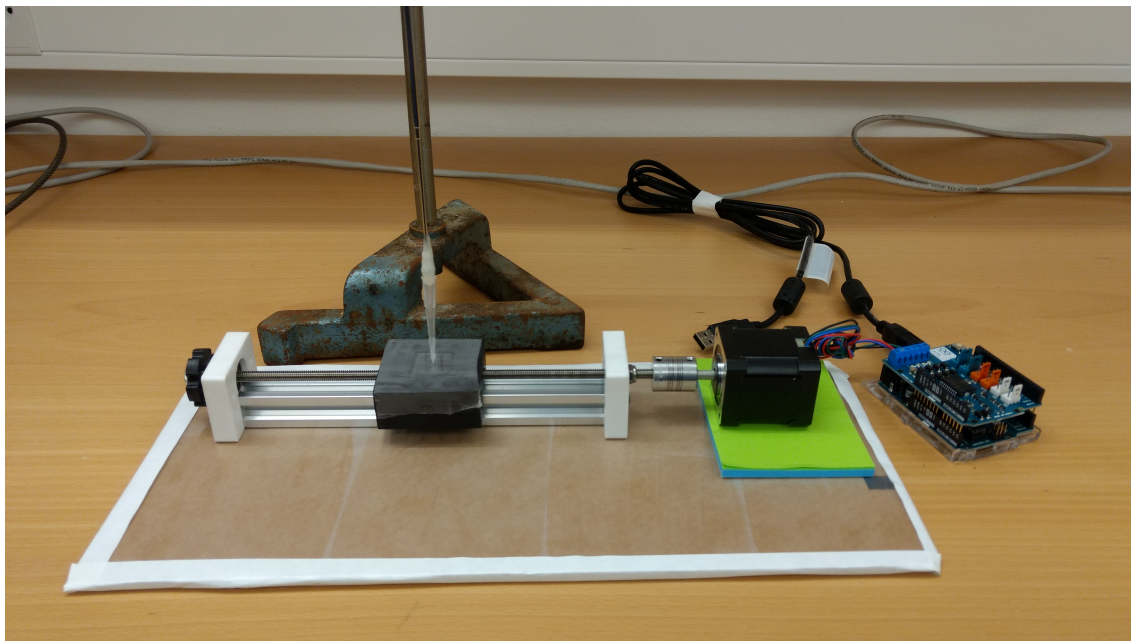


Figure 4.2: Image of the depositor, including stationary pipette tip.

4.1.3 λ -DNA and Plasmid DNA

48.5 kbp long λ -DNA from *Enterobacteria phage* λ , was acquired from Roche Life Science. 150 kbp long DA25168 plasmid DNA was a gift from Linus Sandgren at Uppsala University. All DNA samples taken from stock solutions were diluted and stored in MES-buffer (pH 5.7).

4.1.4 Cleavage of Plasmids Using Cas9 and S1 nuclease

Linearization of plasmids was performed using two endonucleases, Cas9 and S1 nuclease.

Cleavage using Cas9 was performed according to the protocol in Appendix A.1. The enzyme was purchased from PNA Bio, and the RNA was purchased from Dharmacon, GE Life Sciences. The crRNA strand was complementary an NGG sequence 111 on the *bla_{CTX-M-15}gene*, and had the sequence 5' TGCCGAATTA-GAGCGGCAGT 3'. Cleavage using S1 nuclease was performed according to the protocol in Appendix A.2. The enzyme was purchased from Thermo Scientific, and came with relevant buffers.

4.1.5 Fluorescent staining of DNA

YOYO-1 was used as fluorophore. The molar concentration of DNA vs YOYO-1 was kept to 5:1 in all experiments. 200x or 10x solutions (10x means the solution had a 10x higher DNA concentration than the final deposited solution) were prepared according to Table 1. The 10x solution was only used when cutting plasmids with Cas9 due to low concentration in the post-cleavage solution. After incubation at 50° C for 30 min, the solution was diluted to a DNA-concentration of 0.1 μM (except for optimization experiments) and thus ready for deposition.

Table 4.1: Concentrations in the 200x and 10x solutions.

(a) 200xLS		(b) 10xLS	
Substance	Concentration [μM]	Substance	Concentration
DNA	20	DNA	1
YOYO-1	4	YOYO-1	0.2
MES-buffer	Added to a total volume of 10 μl	MES-buffer	Added to a total volume of 10 μl

4.1.6 Deposition

A ZEONEX[®]-coated glass cover slip was placed on the slider of the deposinator, and 2 μl of sample was added on top. A stationary pipette tip was lowered to keep the droplet in place while the slider moved. To ease lowering of the tip, it was fastened to an adjustable radio antenna. The slider was moved 8 mm using the setup to drag the droplet along the cover slip.

4.1.7 Fluorescence Microscopy

The cover slips were taped to a microscope glass for image capture. Zeiss Axio Observer.Z1, equipped with a HBO lamp and a 63x/1.4 TIRF oil immersion objective was used for image capture. The microscope was also equipped with a 1.6x Optovar magnification changer resulting in a total magnification of 100x.

4.2 Experimental Setup

The system was optimized for three parameters (Table 4.2) using deposited λ -DNA.

Early experiments yielded results with heterogeneous fluorescent staining (Figure 4.3). Length estimation is not significantly reliant on homogeneous staining, but it would be an issue if the method were to be used for optical mapping. As the heterogeneous staining was thought to be due to low pH, higher values than 5.7 were tested to assess this hypothesis. pH 5.7 was used by Deen *et al.* (2015) for deposition and was thus set as the lowest value [23]. The system was also evaluated for pH 6.1 and 6.5.

The speed of the deposinator could be controlled, and faster speeds would shorten time needed for experiments. The software controlling the deposinator had



Figure 4.3: Early experiments yielded heterogeneous staining which would affect optical mapping.

three speeds programmed – 2, 10 and 60 mm/min. All three speeds were tested to see the effect of speed on deposition.

Lastly, different concentrations of DNA were tested. If the concentration was high, the DNA molecules would be too closely spaced after deposition which would affect length estimation with the software. DNA concentrations of 0.5, 0.25 and 0.1 μM were tested.

Table 4.2: Parameters optimized for deposition of DNA.

pH	Speed [mm/min]	DNA-conc. [μM]
5.7	2	0.5
6.1	10	0.25
6.5	60	0.1

Table 4.3 shows the various samples that images were taken of. Images of separate samples containing Cas9-cut plasmids, S1 nuclease-cut plasmids, non-cut plasmids and λ -DNA were captured, as well as a sample where λ -DNA was mixed with S1-cut plasmids.

Table 4.3: The different types of samples that were stretched and analysed

λ -DNA
 Non-cut plasmid
 DA25168 cut with S1 nuclease
 λ -DNA+plasmid cut with S1 nuclease
 DA25168 cut with Cas9

4.3 Data processing

This section describes how the lengths of the DNA molecules were estimated after the images had been captured.

4.3.1 Measuring of single DNA molecules

Hemant Kumar, an – at the time – visiting researcher at the Department of Theoretical Physics, Lund University, made a Matlab script that detects and measures the lengths of DNA-molecules in an image. The software had a threshold for minimum number of pixels inside the boundary of a detected molecule. The threshold was meant to reduce noise and can be seen as a high pass filter.

The script formed boundaries around molecules and used three methods for estimating the length. The estimated lengths were then given as a matrix with three

rows. This project used the third method for length estimation, which measured the arc length of the fitted curve of the molecule.

4.3.2 Histogram Plotting

Several images were analysed for each sample, and histograms were made from the results. The values from the results were grouped in whole μm s in the histograms. This means that, for example, molecules measured as 24.8, 25.0 and 25.4 μm would all be rounded to 25 μm .

5

Results and Discussion

5.1 Optimization

To achieve optimal stretching results, and thus allow for more accurate estimations of length, the system was optimized for the following parameters: pH, deposition speed, and concentration. This section presents the results.

5.1.1 pH

The DNA solutions were kept in MES buffer with pH 5.7 to allow binding of the DNA ends to the ZEONEX[®] surface. However, initial results from deposition using pH 5.7 yielded heterogeneous fluorescent staining. Although homogeneous staining is not particularly important for measuring the size of molecules, it would affect barcode quality if the method was utilized for optical mapping.

As there was a possibility that the heterogeneous staining was due to the low pH, higher pH values than 5.7 were tested. Images of the results from deposition of λ -DNA in solution with pH 6.1 and 6.5 is displayed in Figure 5.1. A pH of 6.1 yielded decent stretch of DNA molecules but this was accompanied by noise in the form of bundled up DNA. A pH of 6.5 resulted in poor stretching. The following experiments were thus performed using pH 5.7.

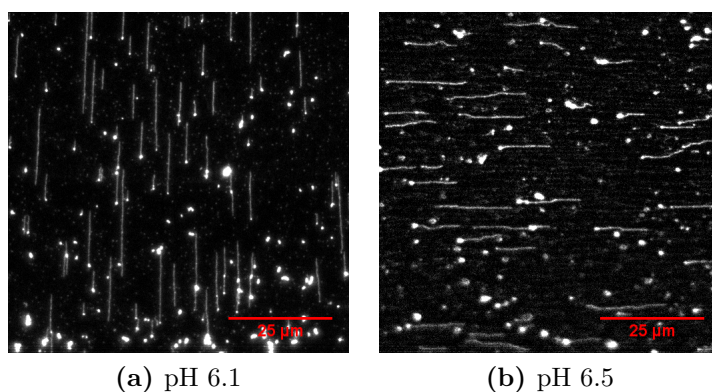


Figure 5.1: Results for $0.1\mu M$ λ -DNA in solution with pH 6.1 and 6.5 deposited on ZEONEX[®]-coated cover slips.

5.1.2 Speed

The software controlling the setup had three settings for speed: 2, 10 and 60 mm/min. 8 mm deposition using 2 mm/min speed thus took 4 minutes. As a higher deposition speed would make the experiments quicker, each speed setting was evaluated to see if there was any difference to DNA-stretching.

Any significant difference to the DNA-stretching was not found between the different speed settings. Lower speed did, however, result in higher amount of DNA deposited. The speed was thus set to 2 mm/min, as to reduce waste of DNA.

Many images had noise in the form of broken DNA fragments. There is a possibility that even lower speeds than 2 mm/min might reduce breakage of DNA molecules and thus reduce noise, but such experiments were not performed due to time constraints. Further, as the software for measuring the molecules was not complete until after experiments were finished, the extent of noise was, at the time of data collection, unknown.

5.1.3 DNA-concentration

The length of the DNA molecules were measured using the Matlab script by Hemant Kumar. Tightly spaced molecules were misinterpreted as one by the script, and deposited DNA molecules thus had to be sufficiently far apart to be discerned as separate molecules. Increasing the distance between molecules was done by decreasing the concentration of DNA in the solutions. Deposition quality depending on concentration was thus evaluated for 0.5, 0.25 and 0.1 μM .

Images of the results from deposition of λ -DNA with different concentrations is displayed in Figure 5.2. A concentration of 0.5 μM proved too high, since many molecules overlapped which would make analysis difficult. A concentration of 0.25 μM yielded less tightly spaced molecules, but there was still a lot of overlap compared to 0.1 μM . The last concentration might be too low and the sweet spot lies somewhere between 0.25 and 0.1 μM . Nevertheless, the following experiments were performed using 0.1 μM to ensure accurate detection with the software.

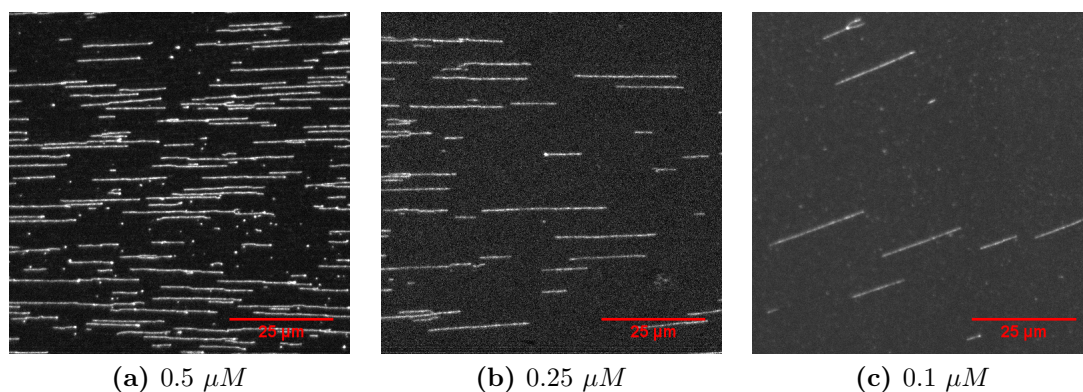


Figure 5.2: 0.5 μM (a), 0.25 μM (b), and 0.1 μM (c) λ -DNA deposited on ZEONEX[®]-coated cover slips.

5.2 Estimation of DNA-length

After optimization, the method was used to estimate the size of the plasmid DA25168. To do this, the stretched lengths of both λ -DNA and DA25168 were measured. As the size of λ -DNA is well known, it should be possible to calculate the size of DA25168 by comparing the λ -length and plasmid length of the stretched molecules.

Measurements were taken from five stretched samples. The software detected and measured lengths of several hundreds molecules in each image. These lengths were used to plot histograms which are presented in this section. The first two samples presented below are deposited DNA from solutions containing only λ -DNA or only non-cut DA25168. To more accurately measure the length of DA25168, the plasmids were linearized according to the S1 protocol in Appendix A.2. Two samples were measured using deposited S1-cut plasmid; one of the samples contained only plasmid, while the other was a mix of λ -DNA and plasmid. The mixed sampled was done to allow comparison in case the stretching differed between different depositions. The final sample contained DA25168 linearized using the Cas9 protocol in Appendix A.1.

It should be noted that the image quality was poor for some samples, and the results are thus less accurate for those samples. The threshold, as mentioned in Section 4.3.1, has been set to 100 pixels for all measurements. This results in a clear drop in number for molecules shorter than $10 \mu m$. What appears to be a peak at this length in some images is thus only due to the threshold.

5.2.1 Length of λ -DNA and Non-cut DA25168

The samples presented in this section were controls. They are two separate samples containing only λ -DNA and only non-cut DA25168.

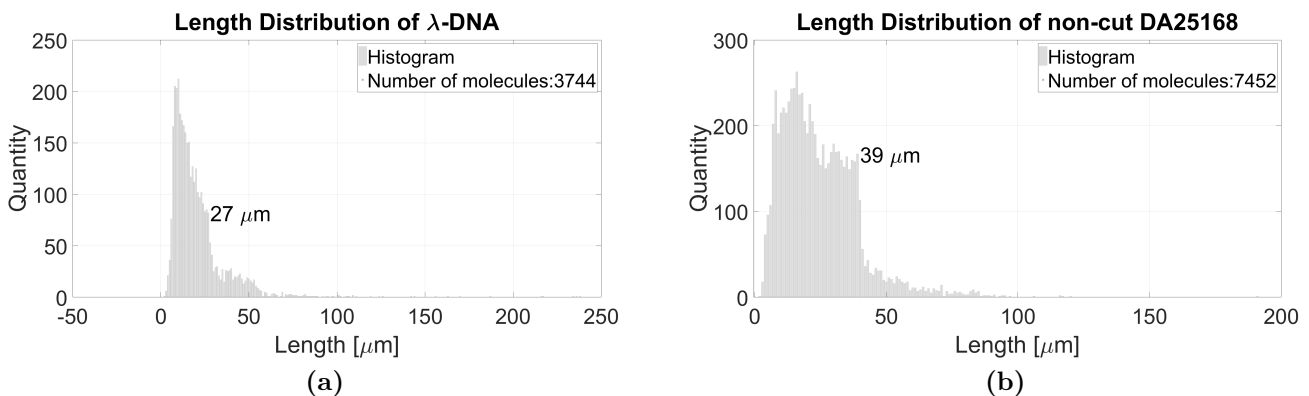


Figure 5.3: (a) Histogram for the length of λ -DNA deposited on a ZEONEX[®]-coated cover slip. (b) Histogram for the length of non-cut DA25168 deposited on a ZEONEX[®]-coated cover slip. A notable drop at $39 \mu m$ has been marked. This is likely about half the length of the plasmid. High resolution versions of both graphs can be found in Appendix B.1.

Figure 5.3(a) shows the histogram for the size of λ -DNA. The λ -DNA had many of broken pieces, but the longer pieces that look nicely stretched seem to be around 25-28 μm , which rhyme well with the histogram. There are no distinct peaks

in the histogram, but there is a drop at $27 \mu m$. The measured lengths below this number are likely due to broken pieces of DNA. Larger molecules could be due to the concatenative nature of λ -DNA.

Figure 5.3(b) displays the histogram for the length of non-cut DA25168. There are no clear peaks in the histogram, but just like with the λ -DNA, there is a distinct drop. This time the drop occurs at $39 \mu m$.

5.2.2 Length of S1-cut DA25168 and S1-cut DA25168 mixed with λ -DNA

The length of DA25168 cut with S1 nuclease was first measured when the plasmid was deposited alone. This was followed by deposition of a sample where the cut plasmid was mixed with λ -DNA. The mixed sample had a concentration of $0.05 \mu M$ for both λ -DNA and DA25168, resulting in a total DNA concentration of $0.1 \mu M$.

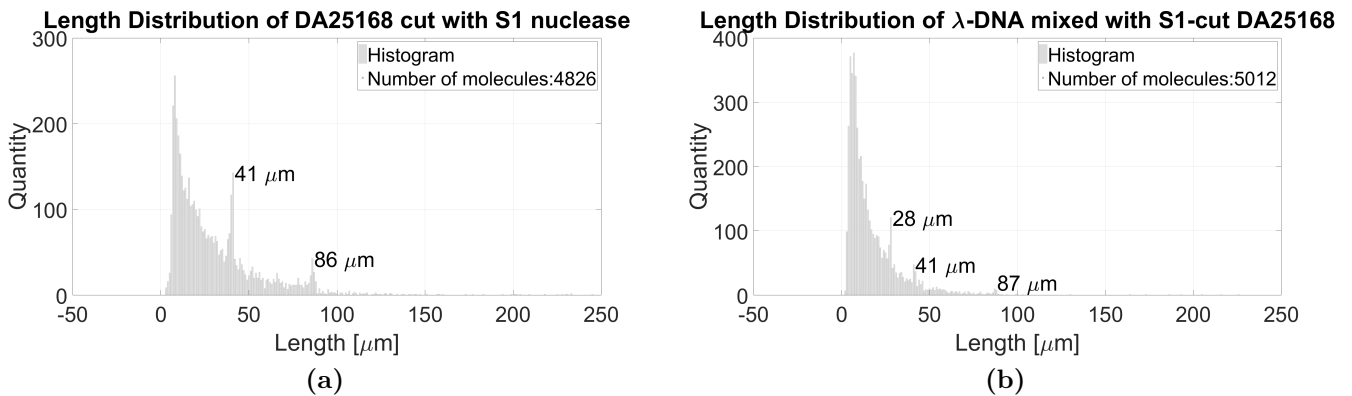


Figure 5.4: (a) Histogram for the length of DA25168 cut with S1 nuclease and deposited on ZEONEX[®]-coated cover slip. Notable peaks have been marked with the corresponding lengths. (b) Histogram for the length of λ -DNA mixed with S1-cut DA25168 deposited on ZEONEX[®]-coated cover slip. Notable peaks have been marked with the corresponding lengths. High resolution versions of both graphs can be found in Appendix B.2.

Figure 5.4(a) displays the histogram for the length of DA25168 cut with S1 nuclease. The histogram has peaks at $41 \mu m$ and $86 \mu m$. There is a very clear noise, which appears to be inversely proportional to the length. Despite the noise, the peaks are clear and the likely length of the plasmid is thus $86 \mu m$. The peak at $41 \mu m$ corresponds well with the non-cut plasmid at $39 \mu m$ and might be due to DNA folding as depicted in Figure 5.5. Folding is especially apparent when stretching non-cut plasmids. The reason to why the DNA folds could be due to intact plasmids breaking during deposition. As a plasmid breaks, both new ends of the molecule could fuse to the ZEONEX[®] at the same spot. Further data would be required to assess this hypothesis.

Figure 5.4(b) displays the histogram for the length of λ -DNA mixed with S1-cut DA25168. The figure can be compared with the S1-cut plasmids in Figure 5.4(a). The same noise and the same two peaks appear, one at $41 \mu m$, and one at $87 \mu m$, but with addition of a third peak at $28 \mu m$. This peak is thus likely the λ -DNA, which corresponds well with the $27 \mu m$ drop in Figure 5.3(a).

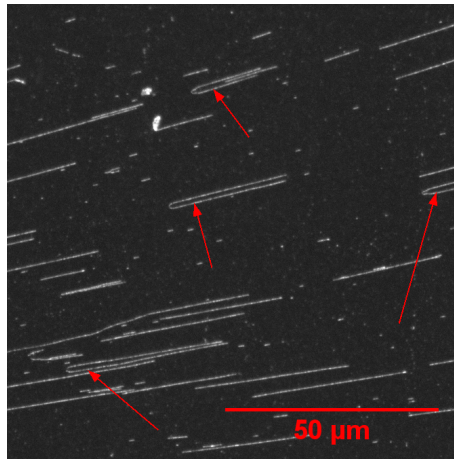


Figure 5.5: The arrows point to examples of folded DNA molecules. These would likely be regarded as one or two molecules each measured as half the true length. The image is from deposited non-cut DA25168, $0.1 \mu M$.

To estimate the base pair-length of the plasmid, a ratio between the measured length (in μm) of λ -DNA and the plasmid can be multiplied with the known length of λ -DNA. Comparing the two peaks, $28 \mu m$ and $87 \mu m$ we end up with a ratio of $\frac{87}{28} = 3.1$. As λ -DNA is 48.5 kbp long, the calculated length of DA25168 is $48.5 \cdot 3.1 = 150.35$ kbp, which matches the expected length of the plasmid.

There is a clear difference between the samples containing only DNA (Figure 5.3) and the samples containing S1 nuclease (Figure 5.4). The samples containing S1 nuclease showed peaks and the only-DNA samples had drops. The reason to this is unknown. Molecules in an S1 solution that have been damaged by stress might have more weak points that are targetable for cleavage, and only intact molecules are left alone. This is highly hypothetical, however, and should be analysed further. Experiments with samples only containing λ -DNA together with S1 nuclease would be able to further assess the significance of the enzyme's effect on noise distribution.

5.2.3 Length of DA25168 cut with Cas9

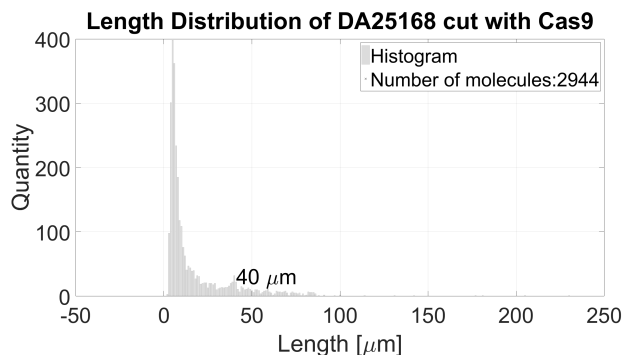


Figure 5.6: Histogram for the length of DA25168 cut with Cas9 and deposited on ZEONEX[®]-coated cover slip. Notable peaks have been marked with the corresponding lengths. High resolution versions of both graphs can be found in Appendix B.3.

The results from the plasmids cut with Cas9 were incontestably the noisiest, as can be seen in Figure 5.6. There is a small peak at 40 μm , but no distinct peak can be observed around 86-87 μm , which was present in the results where the plasmids were cut with S1 nuclease. Further experiments would need to be done to correctly assess the usage of Cas9 for the purpose of length estimation of plasmids deposited on ZEONEX[®].

5.3 Further Discussion

Although the experiments yielded somewhat positive results, the method still holds room for much improvement. This section sums up and extends discussion on questions posed previously in this chapter.

5.3.1 DNA breakage

The first thing to improve before utilizing the method for optical mapping is reduction of noise. A large portion of noise was due to samples having high concentrations of broken DNA. There are three likely factors that induce DNA breakage – deposition speed, external forces, and vibration of the stepper motor.

The stretching of DNA relies on the droplet pulling the molecules with its surface tension, and high speeds of the droplet likely rips the molecules apart. Although the deposition speed was 2 mm/min, DNA molecules are fragile and even such low velocities might induce breakage. It would be simple to assess if lower deposition speed reduce DNA breakage. However, the setup utilizes a stepper motor which divides a full rotation into 400 steps. Although the time for a full rotation might be reduced, the speed between each step would not be smooth at very low speeds. It should be possible to smoothen the rotation by taking half steps or micro steps. Such possibilities should be explored if simply lowering the rotational speed is not sufficient to reduce DNA breakage.

The second factor, external forces, is disruption to the path of the droplet during deposition. As the ZEONEX[®] surface is highly hydrophobic, even small vibrations might shake the droplet and cause breakage of DNA currently being deposited. Fixation of the translation stage on a pressurized microscope table stage might reduce impact from these forces. Some vibration also arises from the stepper motor, and smoothening the steps might reduce this.

The DNA might contain nicks which makes it more sensitive to the stretching. This was however not examined.

5.3.2 Folding

The images of the non-cut plasmids show clear examples of plasmids folding, yielding a drop in the histogram at around half the true size of the DNA molecules. As mentioned, this is likely due to intact plasmids breaking during deposition. The deposition speed might affect this folding, and lower speeds might increase the number of folded molecules. As a plasmid breaks, a low speed might allow time for both ends to fuse simultaneously to the ZEONEX[®] surface, while a high speed might stretch the molecule before both ends have attached. However, lower speeds might reduce the breakage of intact plasmids all together.

It should be noted that no folded plasmids could be found in the sample cut with S1 nuclease. Despite this, there is still a peak at 41 μm which is around half the true size of the molecule. To solely assign the reason for the existence this peak to folded plasmids is thus not accurate. S1 nuclease might nick some supercoiled plasmids at two sites, leaving both sites open for further cleavage. However, there is no apparent reason to why the enzyme would cleave at exactly half the size of the molecule. It could be that the sites sensitive for S1 nicking are the two ends of supercoiled plasmids (Figure 2.5), but such hypotheses are premature. Further, deposition speeds lower than 2 mm/min might decrease the prominence of the 41 μm peak.

5.3.3 Cas9

The Cas9 results left little satisfaction. No clear peak appears at around 86 μm in the histogram, and the one at 40 μm is weak. Comparing the images of plasmids cut with S1 nuclease or Cas9 might shed some light on the issue, however. Figure 5.7 shows two images of the different samples. A common occurrence with the Cas9 cut plasmids is that one of the ends of the DNA molecules is slightly bundled up. This can be seen as fluorescent dots that emit more light than the rest of the molecule. If this occurrence is due to the Cas9 protocol is unknown, and further experiments could confirm or reject this hypothesis. It should be noted that the Cas9 experimental data were gathered about a week earlier than the remaining results, and the experiments were thus performed with hands less skilled with the method.

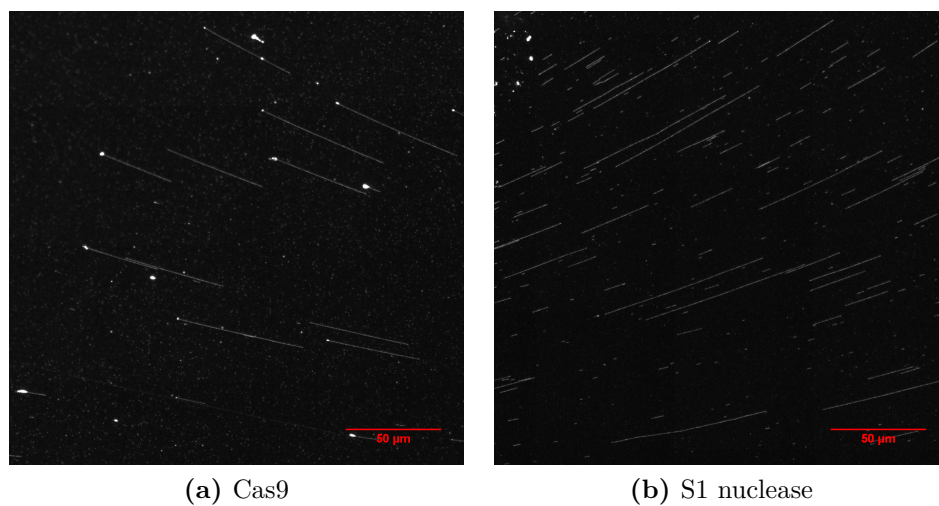


Figure 5.7: Difference between stretched DA25168 cut with Cas9 or S1 nuclease. Dots appear at the ends of some of the plasmids cut with Cas9. This is likely bundled up DNA which could be due to Cas9 interaction.

6

Conclusions

The genetic evolution of bacteria is highly dependent on various types of plasmids. Plasmids have been found to allow spreading of antibiotic resistance between different types of bacteria. To have simple and equipment-light methods for analysis of plasmids is thus important in the fight against antibiotic resistance. This master thesis aimed to optimize and evaluate the usage of a novel molecular combing technique for length estimation of plasmids.

The optimization for the parameters pH, deposition speed, and DNA concentration resulted in pH 5.7, 2 mm/min, and 0.1 μM respectively. Further experiments with lower speed should be performed to assess the effect of deposition speed on DNA breakage.

Length of plasmid DA25168 was accurately estimated to 150 kbp by comparing peaks in the histogram of S1-cut plasmid mixed with λ -DNA. The results were comparable with samples only containing λ -DNA or non-cut plasmid. Histograms from these samples did not have peaks however, but had instead distinct drops. The S1 solutions contained a clear noise, that seemed to be inversely proportional to the length.

DNA breakage was common, and might be reduced by lowering deposition speed and smoothening the steps of stepper motor. Reducing impact of external vibrations could also be done by fastening the setup to an anti-vibration table. It should be noted that experiments carried out by Deen *et al.* using λ -DNA did not contain large amounts of broken DNA, and potential deviations should be analysed.

Cas9 experiments did not yield any significant results, due to poor image quality and ends of plasmids bundling up. New experiments should be performed to truly assess the usage of this enzyme for this purpose.

There might be a possibility to estimate the length from non-cut plasmids as the results yielded a distinct drop at roughly half the size of the plasmid. Some correction factor would probably be needed, and more experiments with various plasmids could assess this. Removing the need of enzymes would simplify experiments in laboratories with limited storage facilities.

To conclude, the method shows promise, but optimization is still required to fully utilize the method for further experimental studies.

Bibliography

- [1] Wikimedia Commons, “File:dna orbit animated static thumb.png,” 2009. [Online; accessed October 12, 2016].
- [2] Wikimedia Commons, “File:base pair at.svg,” 2008. [Online; accessed October 12, 2016].
- [3] Wikimedia Commons, “File:base pair gc.svg,” 2008. [Online; accessed October 12, 2016].
- [4] Wikimedia Commons, “File:eukaryote dna-en.svg,” 2012. [Online; accessed January 11, 2017].
- [5] L. A. Marraffini and E. J. Sontheimer, “Crispr interference: Rna-directed adaptive immunity in bacteria and archaea,” *Nature Reviews Genetics*, vol. 11, no. 3, pp. 181–190, 2010.
- [6] D. Rath, L. Amlinger, A. Rath, and M. Lundgren, “The crispr-cas immune system: Biology, mechanisms and applications,” *Biochimie*, vol. 117, pp. 119–128, 2015.
- [7] Wikimedia Commons, “File:circular dna supercoiling.png,” 2007. [Online; accessed January 12, 2017].
- [8] Wikimedia Commons, “File:tonic water uv.jpg,” 2005. [Online; accessed January 23, 2017].
- [9] Wikimedia Commons, “File:phosphorescence.jpg,” 2008. [Online; accessed January 9, 2017].
- [10] Wikimedia Commons, “File:yoyo-1 fluorescent dye.png,” 2013. [Online; accessed January 13, 2017].
- [11] Wikimedia Commons, “File:fluorescencefilters 2008-09-28.svg,” 2008. [Online; accessed January 23, 2017].
- [12] Wikimedia Commons, “File:stepper motor full step1.png,” 2006. [Online; accessed January 23, 2017].
- [13] Wikimedia Commons, “File:stepper motor full step2.png,” 2006. [Online; accessed January 23, 2017].
- [14] Wikimedia Commons, “File:stepper motor full step3.png,” 2006. [Online; accessed January 23, 2017].
- [15] Wikimedia Commons, “File:stepper motor full step4.png,” 2006. [Online; accessed January 23, 2017].
- [16] P. Tassios, M. Gazouli, E. Tzelepi, H. Milch, N. Kozlova, S. Sidorenko, N. Legakis, and L. Tzouveleki, “Spread of a salmonella typhimurium clone resistant to expanded-spectrum cephalosporins in three european countries,” *Journal of clinical microbiology*, vol. 37, no. 11, pp. 3774–3777, 1999.

- [17] L. Villa, C. Mammina, V. Miriagou, L. S. Tzouveleakis, P. T. Tassios, A. Nastasi, and A. Carattoli, "Multidrug and broad-spectrum cephalosporin resistance among salmonella enterica serotype enteritidis clinical isolates in southern italy," *Journal of clinical microbiology*, vol. 40, no. 7, pp. 2662–2665, 2002.
- [18] K. E. Preston, M. A. Kacica, R. J. Limberger, W. A. Archinal, and R. A. Venezia, "The resistance and integrase genes of pacm1, a conjugative multiple-resistance plasmid, from klebsiella oxytoca," *Plasmid*, vol. 37, no. 2, pp. 105–118, 1997.
- [19] V. Müller and F. Westerlund, "Optical dna mapping in nanofluidic channels: Principles and applications," *Lab on a Chip*, 2017.
- [20] D. Bensimon, A. Simon, V. Croquette, and A. Bensimon, "Stretching dna with a receding meniscus: experiments and models," *Physical review letters*, vol. 74, no. 23, p. 4754, 1995.
- [21] X. Michalet, R. Ekong, F. Fougerousse, S. Rousseaux, C. Schurra, N. Hornigold, M. Van Slegtenhorst, J. Wolfe, S. Povey, J. S. Beckmann, *et al.*, "Dynamic molecular combing: stretching the whole human genome for high-resolution studies," *Science*, vol. 277, no. 5331, pp. 1518–1523, 1997.
- [22] L. K. Nyberg, *Development of methods for optical mapping of nanoconfined DNA*. Chalmers University of Technology, 2015.
- [23] J. Deen, W. Sempels, R. De Dier, J. Vermant, P. Dedecker, J. Hofkens, and R. K. Neely, "Combing of genomic dna from droplets containing picograms of material," *ACS nano*, vol. 9, no. 1, pp. 809–816, 2015.
- [24] V. Müller, F. Rajer, K. Frykholm, L. K. Nyberg, S. Quaderi, J. Fritzsche, E. Kristiansson, T. Ambjörnsson, L. Sandegren, and F. Westerlund, "Direct identification of antibiotic resistance genes on single plasmid molecules using crispr/cas9 in combination with optical dna mapping," *Scientific Reports*, vol. 6, 2016.
- [25] Q. Wei, W. Luo, S. Chiang, T. Kappel, C. Mejia, D. Tseng, R. Y. L. Chan, E. Yan, H. Qi, F. Shabbir, *et al.*, "Imaging and sizing of single dna molecules on a mobile phone," *ACS nano*, vol. 8, no. 12, pp. 12725–12733, 2014.
- [26] A. Kaykov, T. Taillefumier, A. Bensimon, and P. Nurse, "Molecular combing of single dna molecules on the 10 megabase scale," *Scientific reports*, vol. 6, 2016.
- [27] J. D. Watson, F. H. Crick, *et al.*, "Molecular structure of nucleic acids," *Nature*, vol. 171, no. 4356, pp. 737–738, 1953.
- [28] B. Alberts, A. Johnson, J. Lewis, M. Raff, K. Roberts, and P. Walter, *Molecular biology of the cell*. New York: Taylor & Francis, 5th ed., 2008.
- [29] K. E. Preston, C. C. Radomski, and R. A. Venezia, "The cassettes and 3' conserved segment of an integron from klebsiella oxytoca plasmid pacm1," *Plasmid*, vol. 42, no. 2, pp. 104–114, 1999.
- [30] J. A. Meyers, D. Sanchez, L. P. Elwell, and S. Falkow, "Simple agarose gel electrophoretic method for the identification and characterization of plasmid deoxyribonucleic acid.," *Journal of Bacteriology*, vol. 127, no. 3, pp. 1529–1537, 1976.
- [31] F. Casse, C. Boucher, J. Julliot, M. Michel, and J. Denarie, "Identification and characterization of large plasmids in rhizobium meliloti using agarose gel electrophoresis," *Microbiology*, vol. 113, no. 2, pp. 229–242, 1979.

-
- [32] A. Götz, R. Pukall, E. Smit, E. Tietze, R. Prager, H. Tschäpe, J. Van Elsas, and K. Smalla, “Detection and characterization of broad-host-range plasmids in environmental bacteria by pcr.,” *Applied and Environmental Microbiology*, vol. 62, no. 7, pp. 2621–2628, 1996.
- [33] S. V. Rajagopala, S. Casjens, and P. Uetz, “The protein interaction map of bacteriophage lambda,” *BMC microbiology*, vol. 11, no. 1, p. 213, 2011.
- [34] P. Horvath and R. Barrangou, “Crispr/cas, the immune system of bacteria and archaea,” *Science*, vol. 327, no. 5962, pp. 167–170, 2010.
- [35] R. Jansen, J. Embden, W. Gaastra, L. Schouls, *et al.*, “Identification of genes that are associated with dna repeats in prokaryotes,” *Molecular microbiology*, vol. 43, no. 6, pp. 1565–1575, 2002.
- [36] L. Cong, F. A. Ran, D. Cox, S. Lin, R. Barretto, N. Habib, P. D. Hsu, X. Wu, W. Jiang, L. A. Marraffini, *et al.*, “Multiplex genome engineering using crispr/cas systems,” *Science*, vol. 339, no. 6121, pp. 819–823, 2013.
- [37] W. Jiang, D. Bikard, D. Cox, F. Zhang, and L. A. Marraffini, “Rna-guided editing of bacterial genomes using crispr-cas systems,” *Nature biotechnology*, vol. 31, no. 3, pp. 233–239, 2013.
- [38] W. Y. Hwang, Y. Fu, D. Reyon, M. L. Maeder, S. Q. Tsai, J. D. Sander, R. T. Peterson, J. J. Yeh, and J. K. Joung, “Efficient genome editing in zebrafish using a crispr-cas system,” *Nature biotechnology*, vol. 31, no. 3, pp. 227–229, 2013.
- [39] P. Beard, J. F. Morrow, and P. Berg, “Cleavage of circular, superhelical simian virus 40 dna to a linear duplex by s1 nuclease,” *Journal of virology*, vol. 12, no. 6, pp. 1303–1313, 1973.
- [40] B. M. Barton, G. P. Harding, and A. J. Zuccarelli, “A general method for detecting and sizing large plasmids,” *Analytical biochemistry*, vol. 226, no. 2, pp. 235–240, 1995.
- [41] Y. Bai, Z. Yang, M. Qiao, X. Zhang, J. Zhou, and C. Gao, “[the action of s1 nuclease and a cloning strategy for microcircular dnas].,” *Sheng wu gong cheng xue bao = Chinese journal of biotechnology*, vol. 19, no. 2, pp. 240–243, 2003.
- [42] M. A. Chaudhry and M. Weinfeld, “Induction of double-strand breaks by s1 nuclease, mung bean nuclease and nuclease p1 in dna containing abasic sites and nicks,” *Nucleic acids research*, vol. 23, no. 19, pp. 3805–3809, 1995.
- [43] P. Atkins and L. Jones, *Chemical principles: The quest for insight*. Macmillan, 2007.
- [44] P. Atkins, J. De Paula, and R. Friedman, *Quanta, matter, and change: a molecular approach to physical chemistry*. Oxford University Press, 2009.
- [45] B. Valeur and M. N. Berberan-Santos, “A brief history of fluorescence and phosphorescence before the emergence of quantum theory,” *Journal of Chemical Education*, vol. 88, no. 6, pp. 731–738, 2011.
- [46] J. R. Lakowicz, *Principles of fluorescence spectroscopy*. Springer Science & Business Media, 2013.
- [47] E. Wiedemann, “Ueber fluoreszenz und phosphoreszenz i. abhandlung,” *Annalen der Physik*, vol. 270, no. 7, pp. 446–463, 1888.

- [48] S. E. Braslavsky, "Glossary of terms used in photochemistry, (iupac recommendations 2006)," *Pure and Applied Chemistry*, vol. 79, no. 3, pp. 293–465, 2007.
- [49] J. Clayden, W. Warren, N. Greeves, and P. Wothers, *Organic Chemistry*. Oxford University Press, 2001.
- [50] S. Gurrieri, K. S. Wells, I. D. Johnson, and C. Bustamante, "Direct visualization of individual dna molecules by fluorescence microscopy: characterization of the factors affecting signal/background and optimization of imaging conditions using yoyo," *Analytical biochemistry*, vol. 249, no. 1, pp. 44–53, 1997.
- [51] M. L. Bennink, O. D. Schärer, R. Kanaar, K. Sakata-Sogawa, J. M. Schins, J. S. Kanger, B. G. de Groot, and J. Greve, "Single-molecule manipulation of double-stranded dna using optical tweezers: interaction studies of dna with reca and yoyo-1," *Cytometry*, vol. 36, no. 3, pp. 200–208, 1999.
- [52] D. Marie, D. Vaultot, and F. Partensky, "Application of the novel nucleic acid dyes yoyo-1, yo-pro-1, and picogreen for flow cytometric analysis of marine prokaryotes.," *Applied and environmental microbiology*, vol. 62, no. 5, pp. 1649–1655, 1996.
- [53] C. Carlsson, A. Larsson, M. Jonsson, B. Albinsson, and B. Norden, "Optical and photophysical properties of the oxazole yellow dna probes yo and yoyo," *The Journal of Physical Chemistry*, vol. 98, no. 40, pp. 10313–10321, 1994.
- [54] A. S. Biebricher, I. Heller, R. F. Roijmans, T. P. Hoekstra, E. J. Peterman, and G. J. Wuite, "The impact of dna intercalators on dna and dna-processing enzymes elucidated through force-dependent binding kinetics," *Nature communications*, vol. 6, 2015.
- [55] H. S. Rye, S. Yue, D. E. Wemmer, M. A. Quesada, R. P. Haugland, R. A. Mathies, and A. N. Glazer, "Stable fluorescent complexes of double-stranded dna with bis-intercalating asymmetric cyanine dyes: properties and applications," *Nucleic acids research*, vol. 20, no. 11, pp. 2803–2812, 1992.
- [56] L. K. Nyberg, F. Persson, J. Berg, J. Bergström, E. Fransson, L. Olsson, M. Persson, A. Stålnacke, J. Wiggenius, J. O. Tegenfeldt, *et al.*, "A single-step competitive binding assay for mapping of single dna molecules," *Biochemical and biophysical research communications*, vol. 417, no. 1, pp. 404–408, 2012.
- [57] L. Nyberg, F. Persson, B. Åkerman, and F. Westerlund, "Heterogeneous staining: a tool for studies of how fluorescent dyes affect the physical properties of dna," *Nucleic acids research*, vol. 41, no. 19, pp. e184–e184, 2013.

A

Protocols

A.1 Cas9 Cleavage

This section describes the protocol for cleavage of plasmids using Cas9.

1. The following reaction mixture was prepared in a tube.

Substance	Volume	Stock Concentration
crRNA	5 μ l	100 μ M
tracrRNA	5 μ l	100 μ M
NEB Buffer 3	1.5 μ l	10X
BSA	0.75 μ l	20X
Tris-EDTA Buffer 3	2.75 μ l	10 mM

Incubation at 4° C for 30 min.

2. The following reaction mixture was prepared in a **new** tube.

Substance	Volume	Stock Concentration
Solution from 1	1.5 μ l	
Cas9	0.6 μ l	1000 ng/ μ l
NEB Buffer 3	0.35 μ l	10X
BSA	0.18 μ l	20X
Tris-EDTA Buffer 3	2.37 μ l	10 mM

Incubation at 37° C for 15 min.

3. The following substances were added to a the tube from **2**.

Substance	Volume	Stock Concentration
Plasmid DNA	1.15 μ l (60 ng)	52.2 ng/ μ l
NEB Buffer 3	1 μ l	10X
BSA	0.5 μ l	20X
Tris-EDTA Buffer 3	to a final volume of 15 μ l	10 mM

Incubation at 37° C for 60 min. Final DNA concentration: 6.5 μ M

A.2 S1 nuclease Cleavage

This section describes the protocol for cleavage of plasmids using S1 nuclease.

1. The following reaction mixture was prepared in a tube.

Substance	Volume	Stock Concentration
Plasmid DNA	1.92 μ l (60 ng)	52.2 ng/ μ l
Reaction buffer for S1 nuclease	3 μ l	5X
S1 nuclease	0.1 μ l	10 U/ μ l
MQ water	to a final volume of 30 μ l	

Incubation at RT for 30 min.

2. Stop the reaction by adding 2 μ l of 0.5 M EDTA and heating at 70° C for 10 min.

NOTE: The S1 nuclease was provided as a 100 U/ μ l stock but was diluted with 1X reaction buffer immediately prior to use.

B

High Resolution Histograms

B.1 Figure 5.3

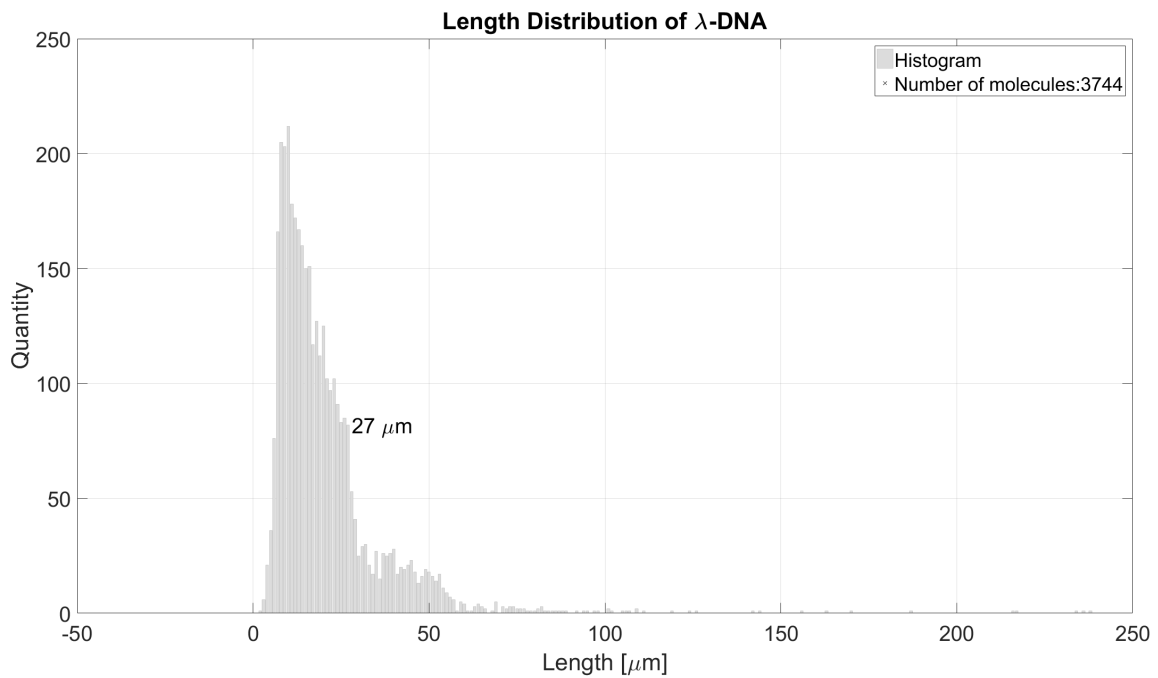


Figure B.1: High resolution histogram for the length of λ -DNA deposited on ZEONEX[®]-coated cover slip.

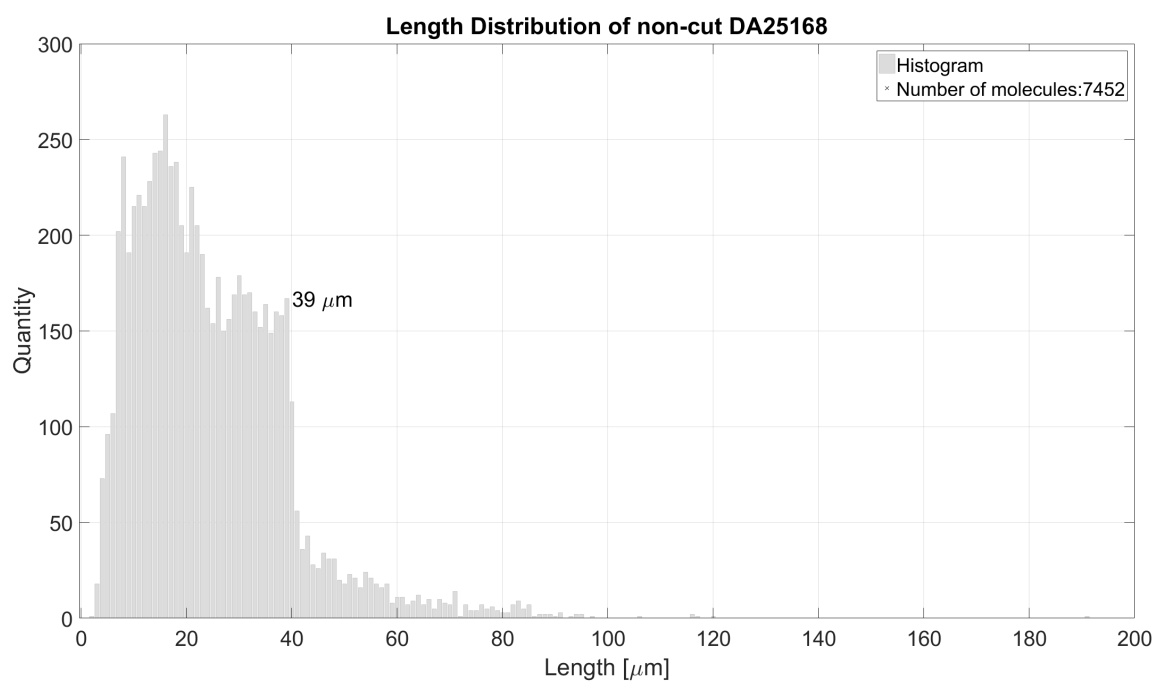


Figure B.2: High resolution histogram for the length of non-cut DA25168 deposited on ZEONEX[®]-coated cover slip. A notable drop at 39 μm has been marked. This is likely about half the length of the plasmid.

B.2 Figure 5.4

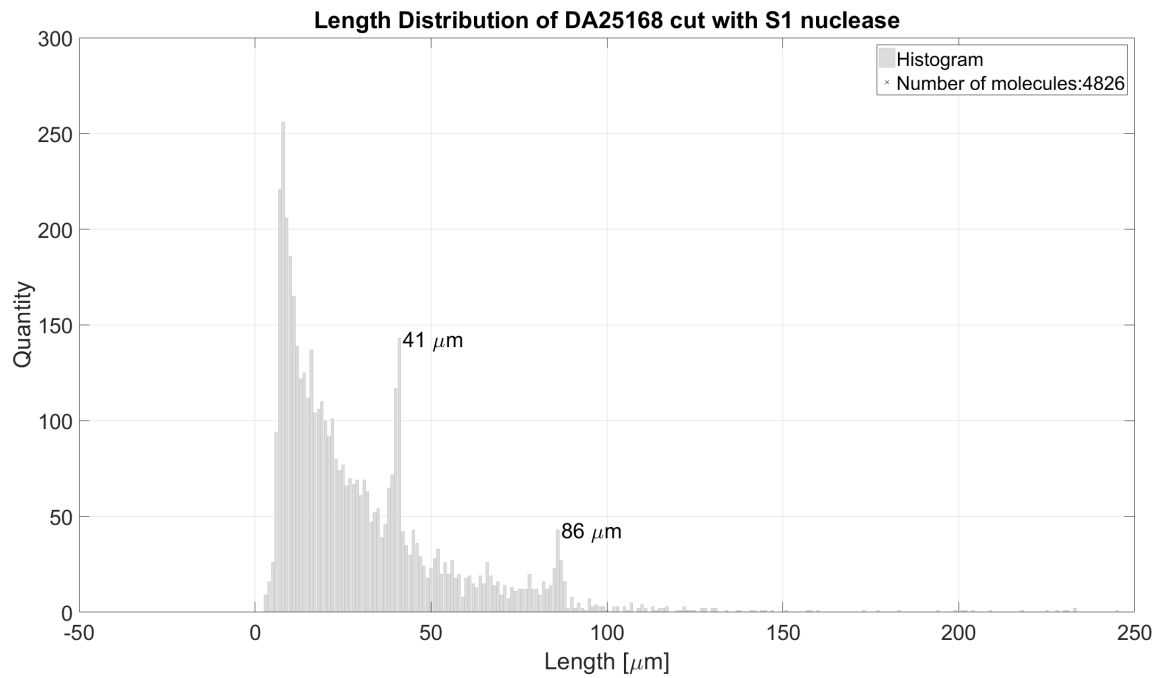


Figure B.3: Histogram for the length of DA25168 cut with S1 nuclease and deposited on ZEONEX[®]-coated cover slip. Notable peaks have been marked with the corresponding lengths.

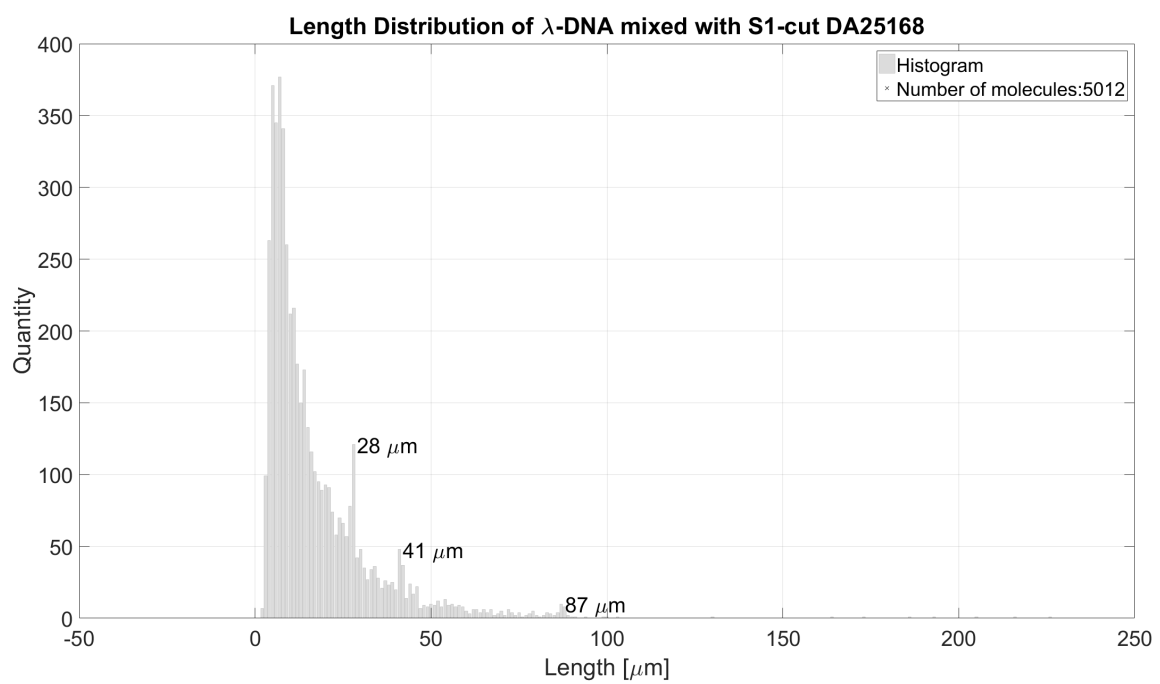


Figure B.4: Histogram for the length of λ -DNA mixed with S1-cut DA25168 deposited on ZEONEX[®]-coated cover slip. Notable peaks have been marked with the corresponding lengths.

B.3 Figure 5.6

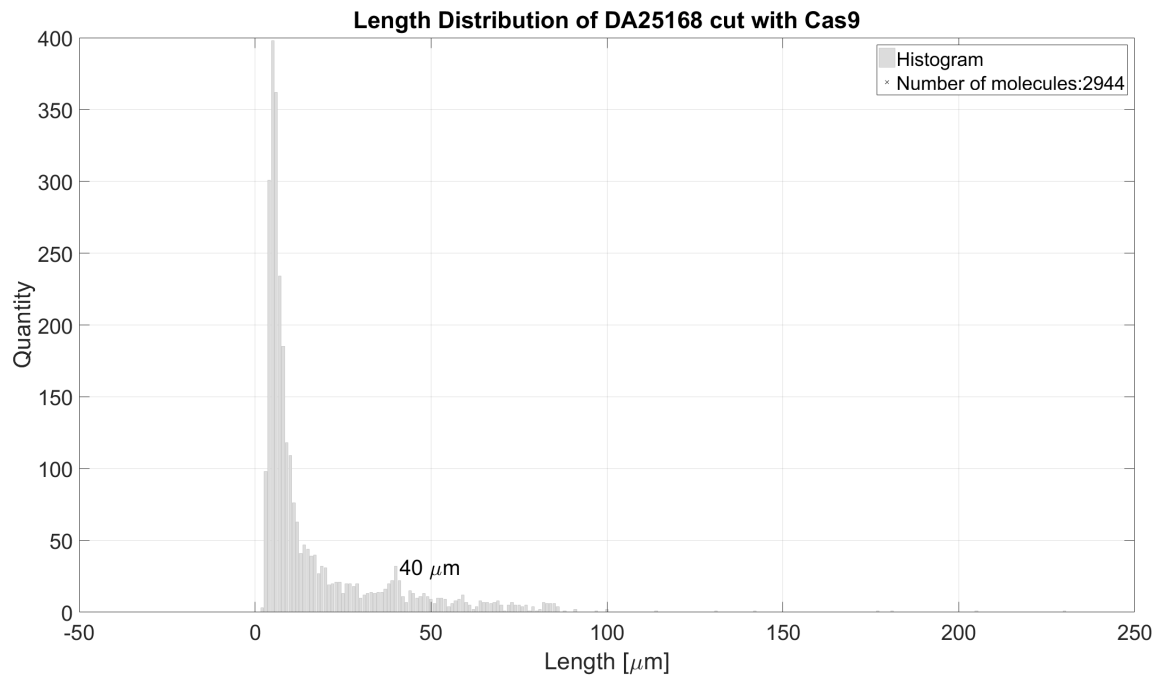


Figure B.5: Histogram for the length of DA25168 cut with Cas9 and deposited on ZEONEX[®]-coated cover slip. Notable peaks have been marked with the corresponding lengths.